

Withaferin A in combination with Cisplatin suppresses mucin family proteins in Epithelial Ovarian Cancer Cells

Jenna Chong, Surinder Batra, Mariusz Ratajczak, Sham S Kakar

Departments of Physiology and Biophysics, James Graham Brown Cancer Center, University of Louisville

Abstract

Ovarian cancer is the leading cause of death among gynecological cancers and is the fifth leading cause of cancer death in women. Currently, ovarian cancer is diagnosed with MUC 16 (CA-125), a transmembrane glycoprotein, used as a serum biomarker. Initially, ovarian cancer is treated with a combination of cytoreductive surgery and platinum/taxane combination chemotherapy which is effective in 70-80% of the cases. After first round of treatment, serum MUC 16 level is a good indicator of survival. An increase in MUC 16 level in serum indicates recurrent epithelial ovarian cancer in which platinum/taxane based chemotherapy is only 30% effective. Various investigators have reported that the mucin family, particularly MUC 1, 4 and 16 in ovarian cancer play a role in not just cancer cell proliferation but also metastasis which may be part of reoccurrence of cancer. **We hypothesize that Withaferin A in combination with Cisplatin can sensitize EOC to cisplatin as a result of down regulation of expression of MUC 1, MUC 4 and MUC 16.** In the present study, we studied the effects of Withaferin A (WFA), cisplatin (CIS) both alone and in combination on expression of MUC1, MUC4 and MUC16 both in epithelial ovarian cancer cell line A2780 and orthotopic ovarian tumors generated in mice by injecting A2780 cells directly into ovaries. Western blot and immunohistochemical analysis were used to determine the expression of MUC 1, MUC 4 and MUC 16. Immunohistochemical and western blot analysis revealed that cisplatin alone increases the expression of MUC 16 in A2780 cells as well as in ovarian tumors and MUC 1 and MUC 4 in ovarian tumors. In contrast, WFA alone and in combination with Cisplatin suppressed the expression of MUC 1, MUC 4 and MUC 16 in A2780 cells as well as in tumors. Combination of WFA and CIS was found to be highly effective in suppression of MUC 1, MUC 4 and MUC 16, suggesting that the WFA and CIS combination therapy may be a potential therapy for ovarian cancer.

Role of Mucins in Ovarian Cancer

MUC1, MUC 4 and MUC 16 are heavily glycosylated transmembrane proteins that have 2 main regions:

- N-terminal subunit containing glycosylated tandem repeats contributes to mucous gels
- C-terminal subunit containing PTS repeats

Release of glycosylated tandem repeats from the N-terminal subunit contributes to mucous gels. Glycocalyx. C-terminal transmembrane subunits function as receptors for cell signaling.

MUC 1

- Cell aggregation and adhesion by affecting E-cadherin [1]
- Cell growth and proliferation by affecting cell signaling pathways within cell [5]

MUC 4

- Affects EMT by decreasing expression of E-cadherin and CK18, increasing expression of N-cadherin and vimentin
- Increasing expression of EMT transcription factors (TWIST1/2, SNAIL) [2]

MUC 16

- Peritoneal metastasis by interacting with mesothelin [3]
- Immunosuppressive traits:
 - Inhibit NK cell response
 - Down regulate CD16 [4]

Results

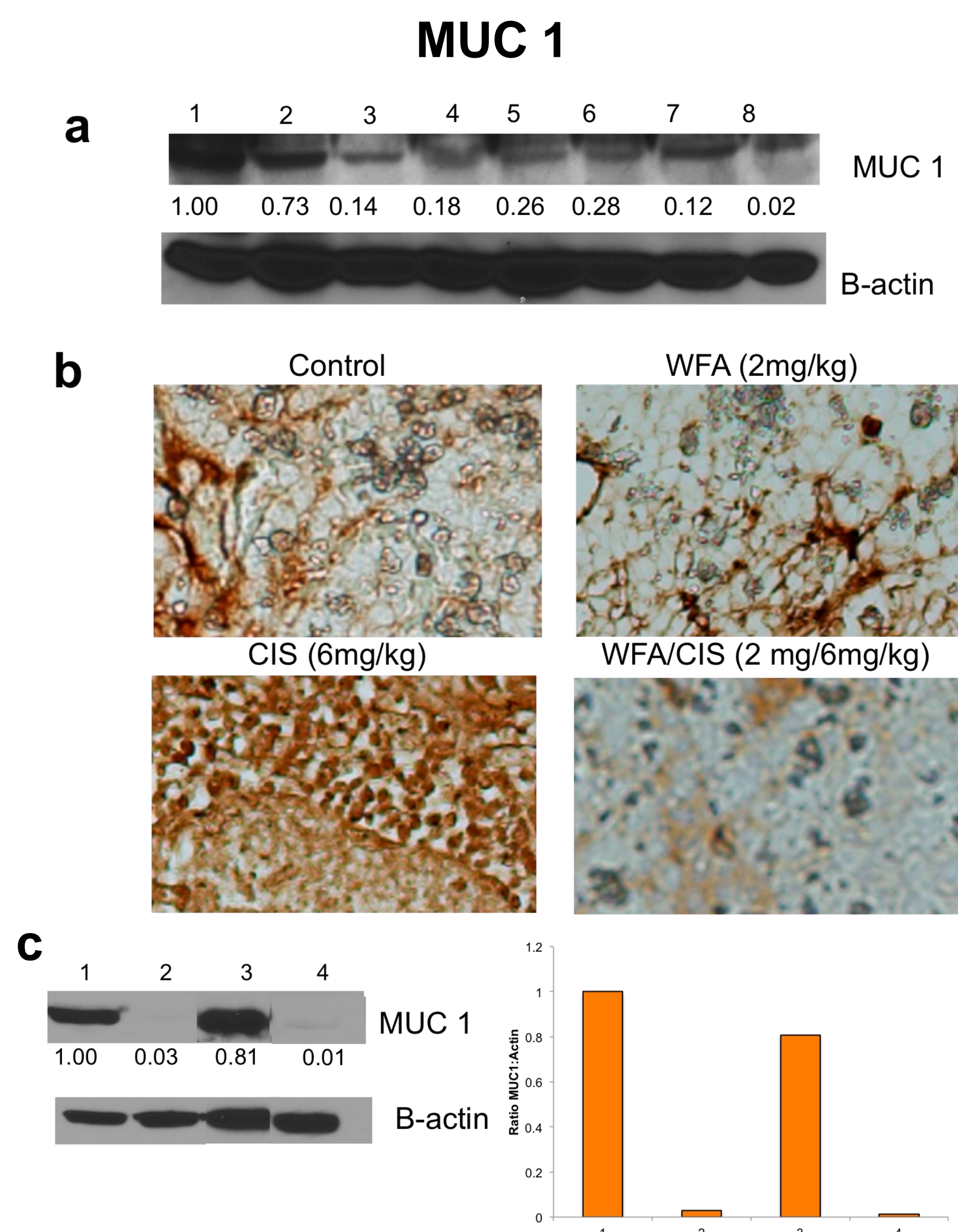


Fig 1. MUC 1 expression in (a) A2780 Cell line treated with WFA, Cis or Combination [Lane 1. Control, 2. WFA 0.5 uM, 3. WFA 1.5 uM, 4. WFA 5.0 uM, 5. CIS 20 uM, 6. CIS 100 uM, 7. WFA 1.5 uM + CIS 20uM, 8. WFA 1.5 uM + CIS 20 uM] (b) Ovarian tumor sections isolated from nude mice treated with WFA, CIS or combination (c) Ovarian tumor [Lane 1. Control, 2. WFA 2 mg/kg, 3. CIS 6 mg/kg, 4. WFA 2mg/kg + CIS 6 mg/kg].

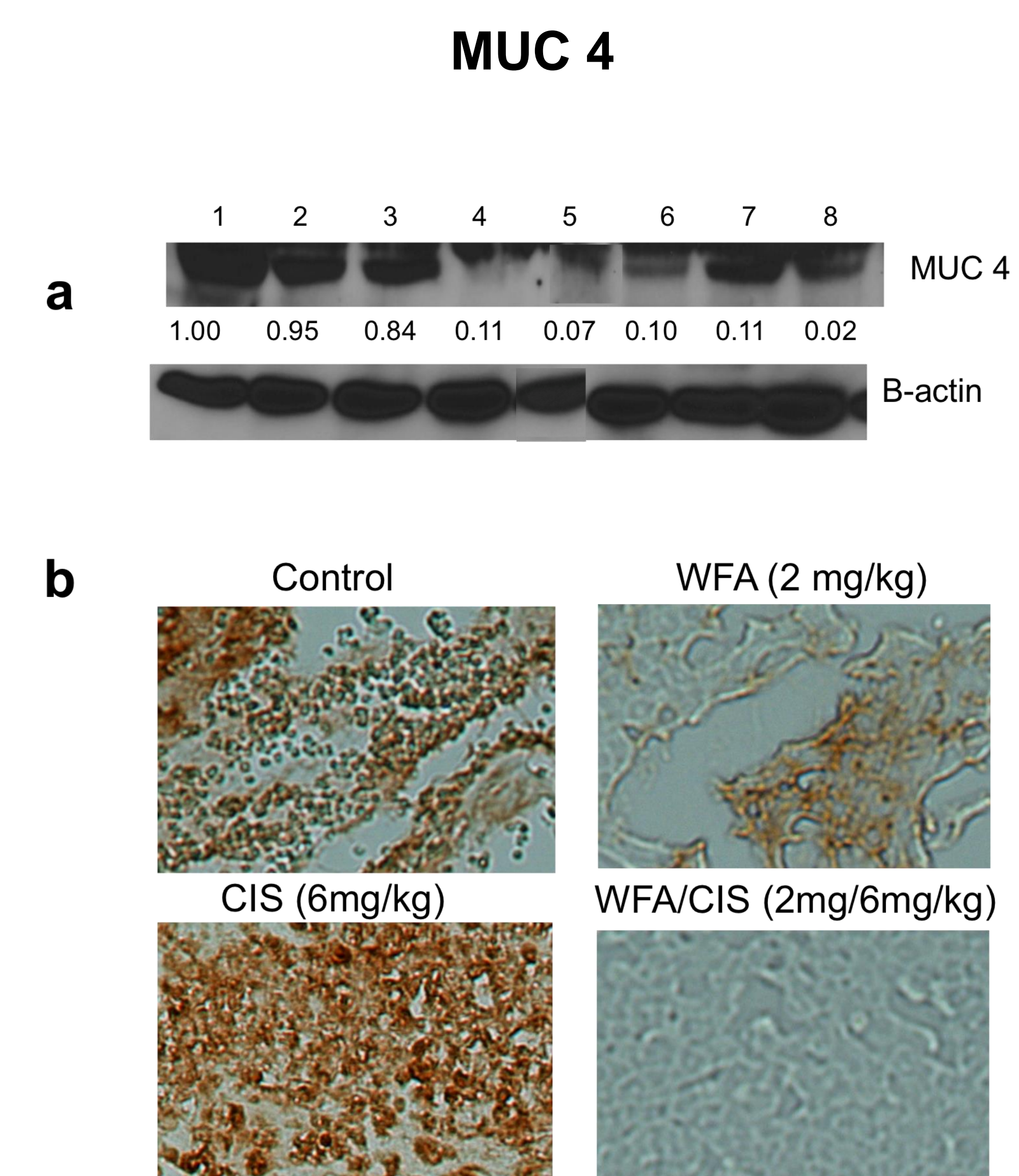


Fig 2. MUC 4 expression in (a) A2780 Cell line treated with WFA, Cis or Combination [Lane 1. Control, 2. WFA 0.5 uM, 3. WFA 1.5 uM, 4. WFA 5.0 uM, 5. CIS 20 uM, 6. CIS 100 uM, 7. WFA 1.5 uM + CIS 20uM, 8. WFA 1.5 uM + CIS 20 uM] (b) Ovarian tumor sections isolated from nude mice treated with WFA, CIS or combination

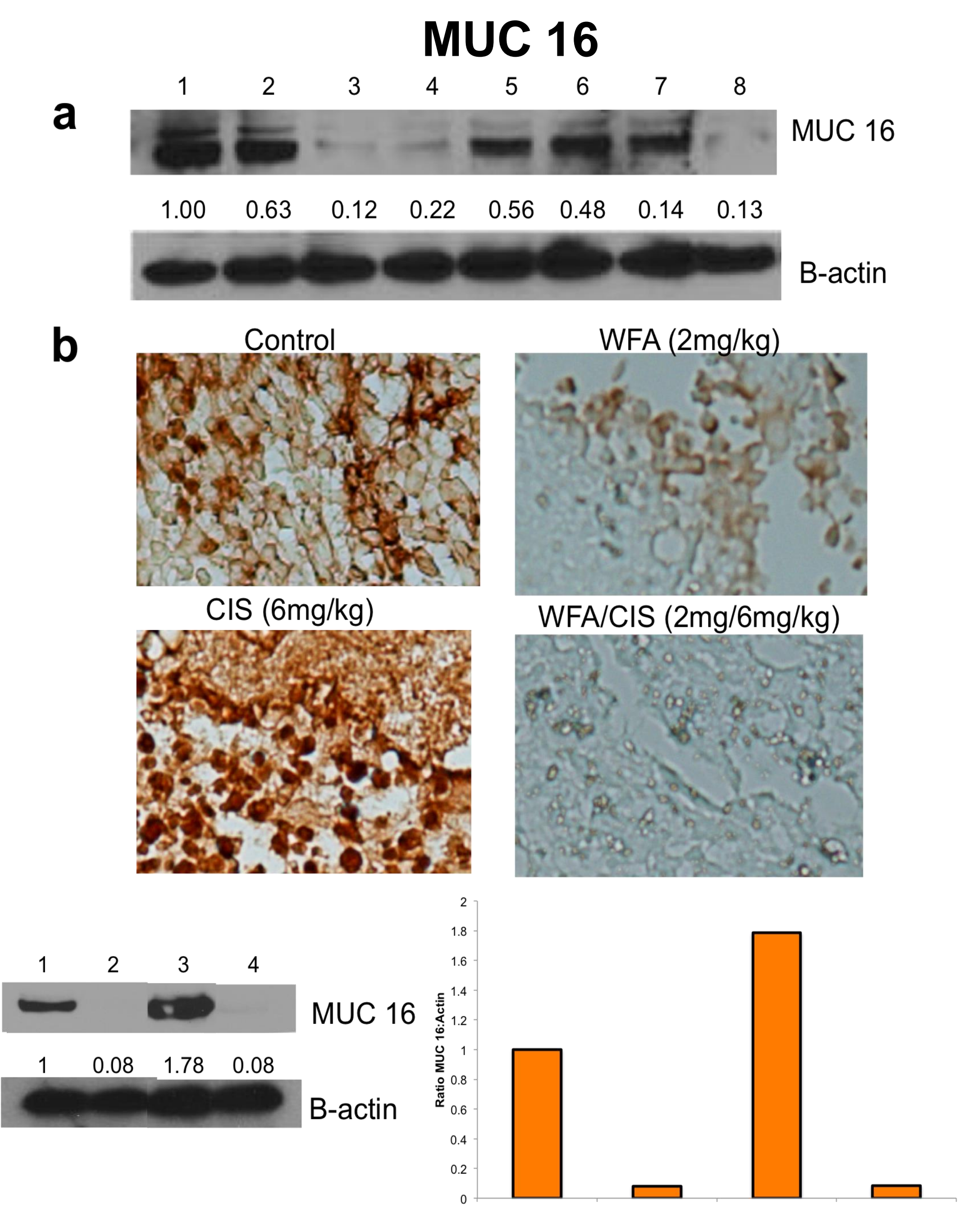
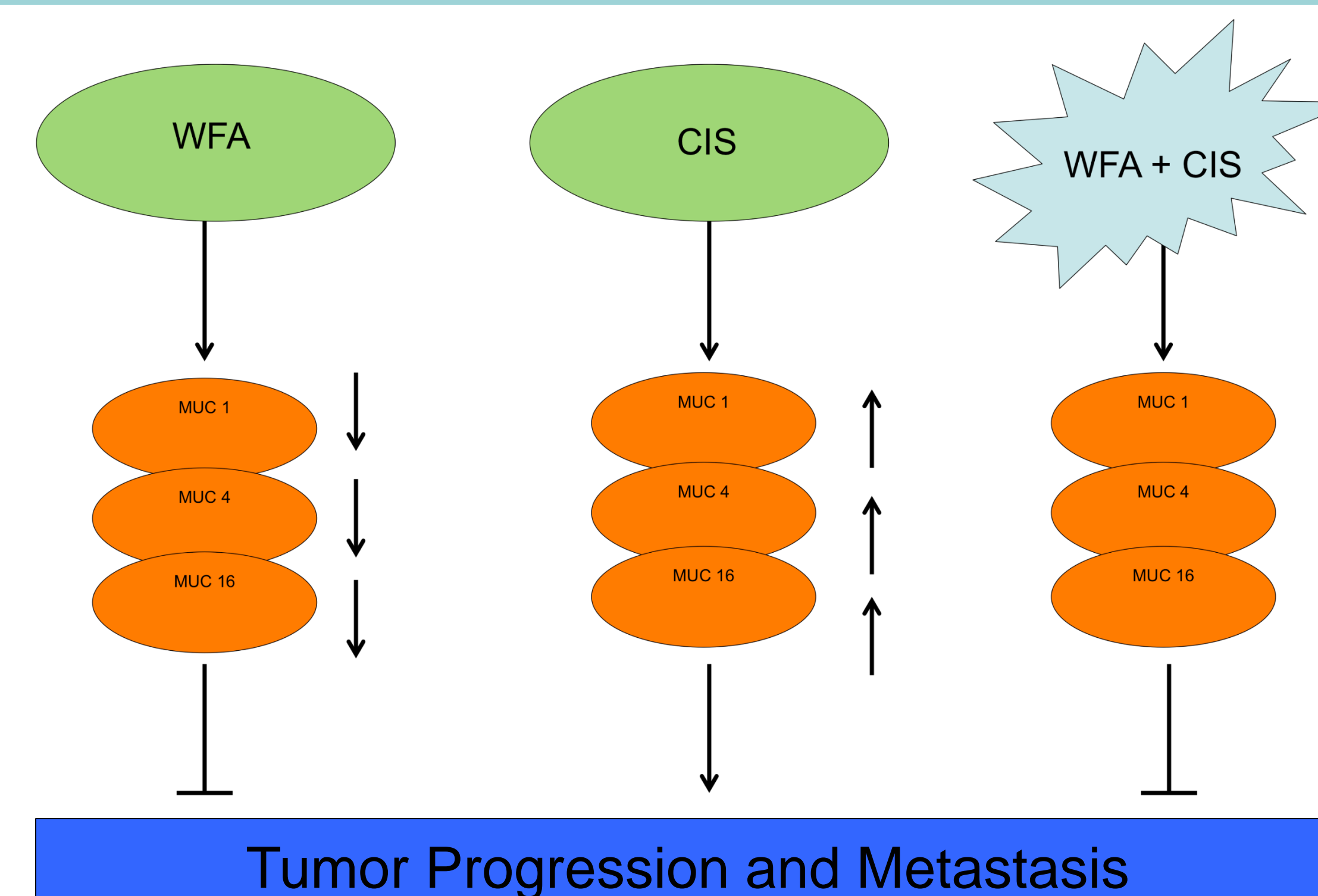


Fig 3. MUC 16 expression in (a) A2780 Cell line treated with WFA, Cis or Combination [Lane 1. Control, 2. WFA 0.5 uM, 3. WFA 1.5 uM, 4. WFA 5.0 uM, 5. CIS 20 uM, 6. CIS 100 uM, 7. WFA 1.5 uM + CIS 20uM, 8. WFA 1.5 uM + CIS 20 uM] (b) Ovarian tumor sections isolated from nude mice treated with WFA, CIS or combination (c) Ovarian tumor [Lane 1. Control, 2. WFA 2 mg/kg, 3. CIS 6 mg/kg, 4. WFA 2mg/kg + CIS 6 mg/kg].

Conclusion

- Withaferin A alone and in combination with Cisplatin decreases expression of MUC 1, MUC 4, and MUC 16
- Cisplatin alone increases the expression of MUC1, MUC 4 and MUC 16 in orthotopic tumors by increasing number of cancer cells expressing each gene.
- Combination of Withaferin A and Cisplatin at higher concentration significantly decreases expression of MUC 1, MUC 4 and MUC 16 in orthotopic tumors and A2780 cell line.
- Combination of Withaferin A and Cisplatin at higher concentrations decreases expression of MUC 1, MUC 4 and MUC 16 and is correlated with a decrease in cancer stem cells [6]
- Withaferin A and Cisplatin may work through MUC members to decrease cancer stem cells as shown by previous study [6]



References

- Kondo K, Kohno N, Yokoyama A, Hiwada K. Decreased MUC1 expression induces E-cadherin-mediated cell adhesion of breast cancer cell lines. *Cancer Res.* 1998;58:2014-2019
- Ponnusamy MP, Lakshmanan L, Jain M, Das S, Chakraborty S, Dey P, Batra SK. MUC4 mucin-induced epithelial to mesenchymal transition: a novel mechanism for metastasis of human ovarian cancer cells. *Oncogene* 2010 (42):5741-54.
- Rump A, Morikawa Y, Tanaka A, Minami S, Umesaki N, Takeuchi M, Miyajama A. Binding of ovarian cancer antigen CA125/MUC16 to mesothelin mediates cell adhesion. *J Biol Chem.* 2004; 279:9190-9198.
- Belisle JA, Gubbels JA, Raphael CA, Migneault M, Rancourt C, Connor JP, Patankar MS. Peritoneal natural killer cells from epithelial ovarian cancer patients show an altered phenotype and bind to the tumour marker MUC 16. *(CA125) Immunology.* 2007; 122:418-429.
- Hollingsworth MA, Swanson BJ. Mucins in cancer: protection and control of the cell surface. *Nat Rev Cancer.* 2004;4:45-60.
- Kakar SS, Ratajczak MZ, Powell KS, Moghadamfalahi M, Miller DM, Batra SK, et al. (2014) Withaferin A Alone and in Combination with Cisplatin Suppresses Growth and Metastasis of Ovarian Cancer by Targeting Putative Cancer Stem Cells. *PLoS ONE* 9(9): e107596.

Acknowledgements

National Cancer Institute grant R25-CA134283
Kakar Lab – Taylor Johnson & Ria Jain



A CRISPR/Cas9 SYSTEM TO EDIT RAT *Mcs1b* CANDIDATE CAUSAL VARIANTS

Thomas Gordon III, Alissa Doll, Saasha Kareparembil, David Samuelson

Department of Biochemistry and Molecular Genetics
University of Louisville School of Medicine

Introduction

- In the 1990s, two major cancer susceptibility genes were identified for breast cancer: BRCA1 and BRCA2. After a point, genetic linkage studies in high incidence breast cancer families did not identify any more predisposing mutations. (Source)
- Studies have been conducted testing the cancer suppressing effect of a rat quantitative trait locus (QTL) named *Mammary carcinoma susceptibility 1b (Mcs1b)*
- Mapping and sequencing of the *Mcs1b* QTL have revealed candidate causal variants.
- CRISPR/Cas9, or Clustered Regularly Interspaced Short Palindromic Repeats/Cas9, is an RNA-guided nuclease bacterial system involved in the defense against invading phages and plasmids.
- The CRISPR/Cas9 system can be engineered to facilitate genome editing in mammalian cells. The Cas9 nuclease enzyme can make double stranded breaks at specific locations in the DNA because guide RNAs (gRNAs) recruit the nuclease to cut at specific genomic locations.
- These double-strand breaks in DNA may be repaired by non-homologous end joining (NHEJ) DNA-repair. NHEJ repair often results in insertion or deletion mutations.
- Cells can also use an alternative repair system to correctly repair itself, which is typically less error prone, called homology-directed repair.

Hypothesis

Candidate variant A74-UL-SNV-18 is involved in regulating transcript levels of *Mcs1b* genes.

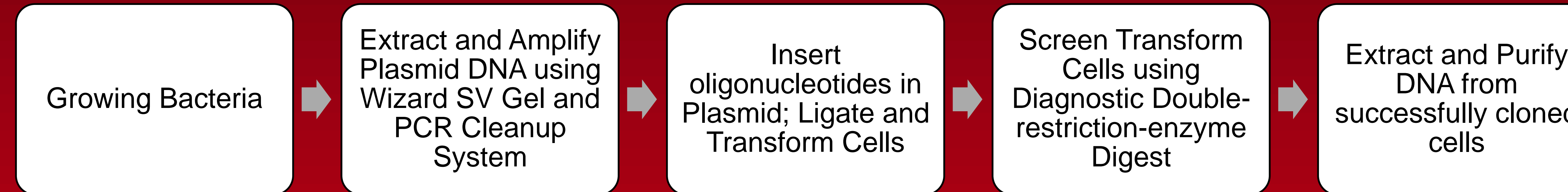
Objective

- Successfully clone plasmids containing gRNA sequences designed to target A74-UL-SNV-18.

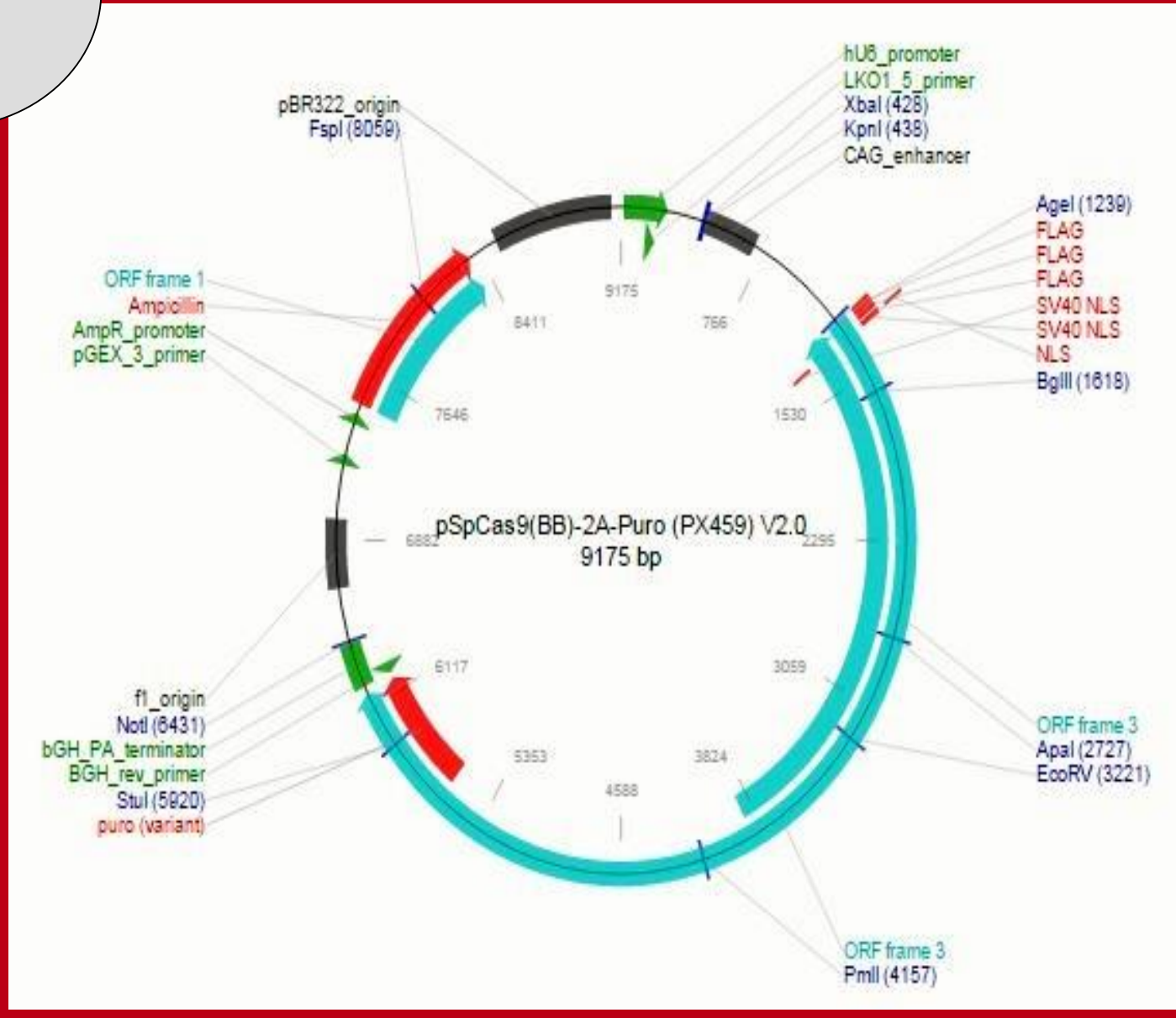
Translational Relevance

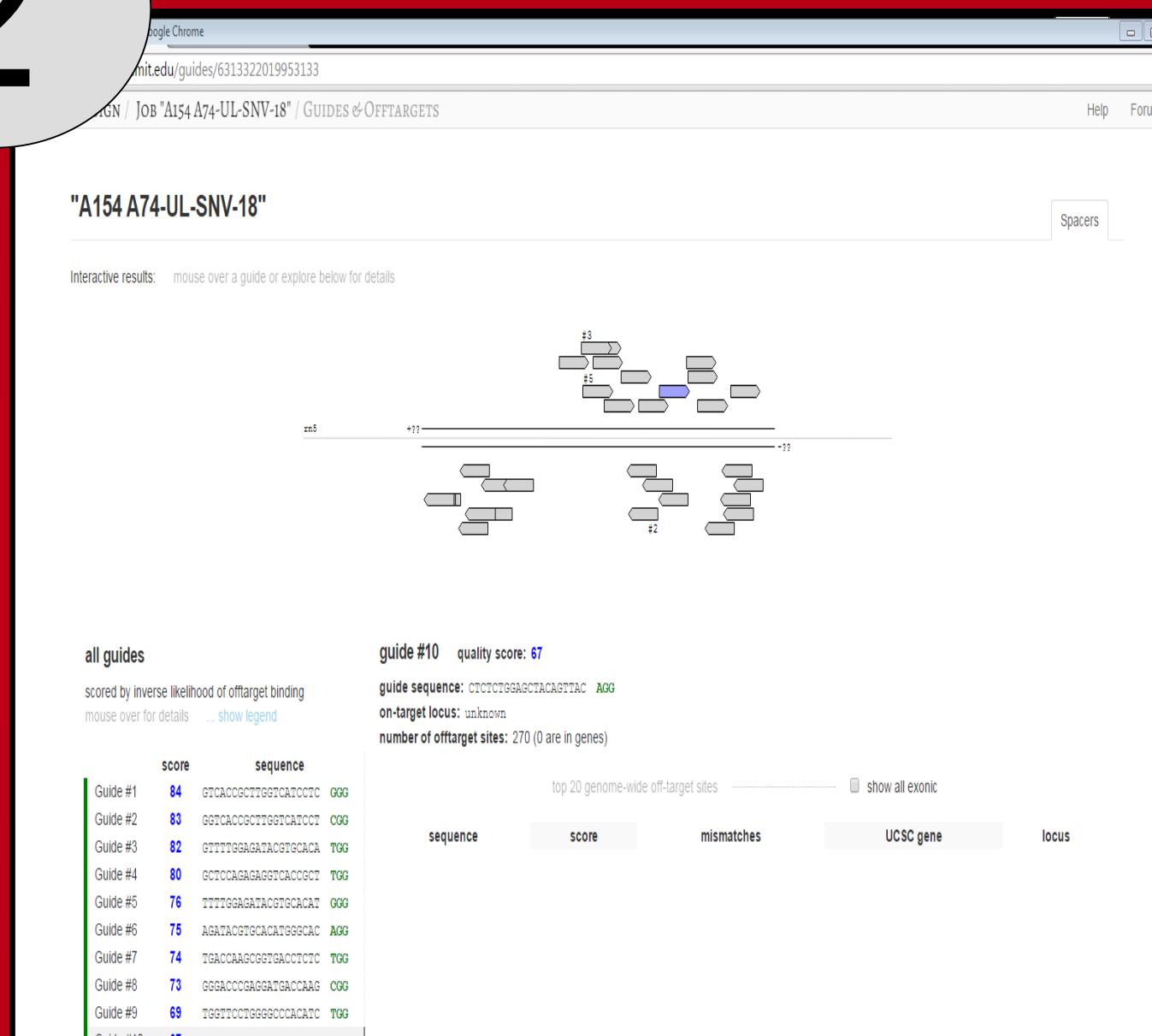
Rat *Mcs1b* is orthologous to breast cancer risk associated human locus 5q11.2. Understanding this locus in rats could help to understand breast cancer risk in humans. Further, this work could also identify potential breast cancer prevention pathways.

Methods



Results

1 

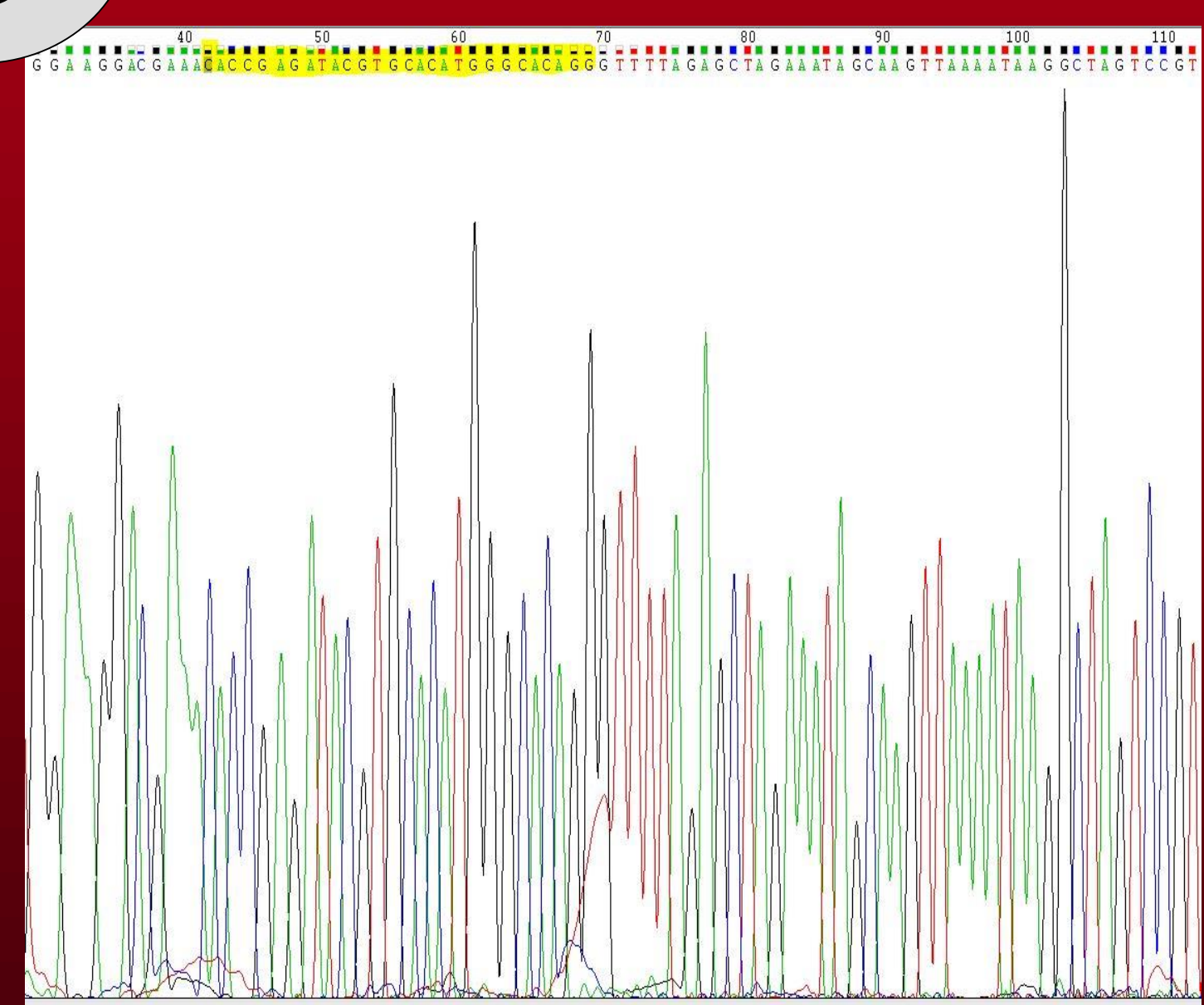
2 

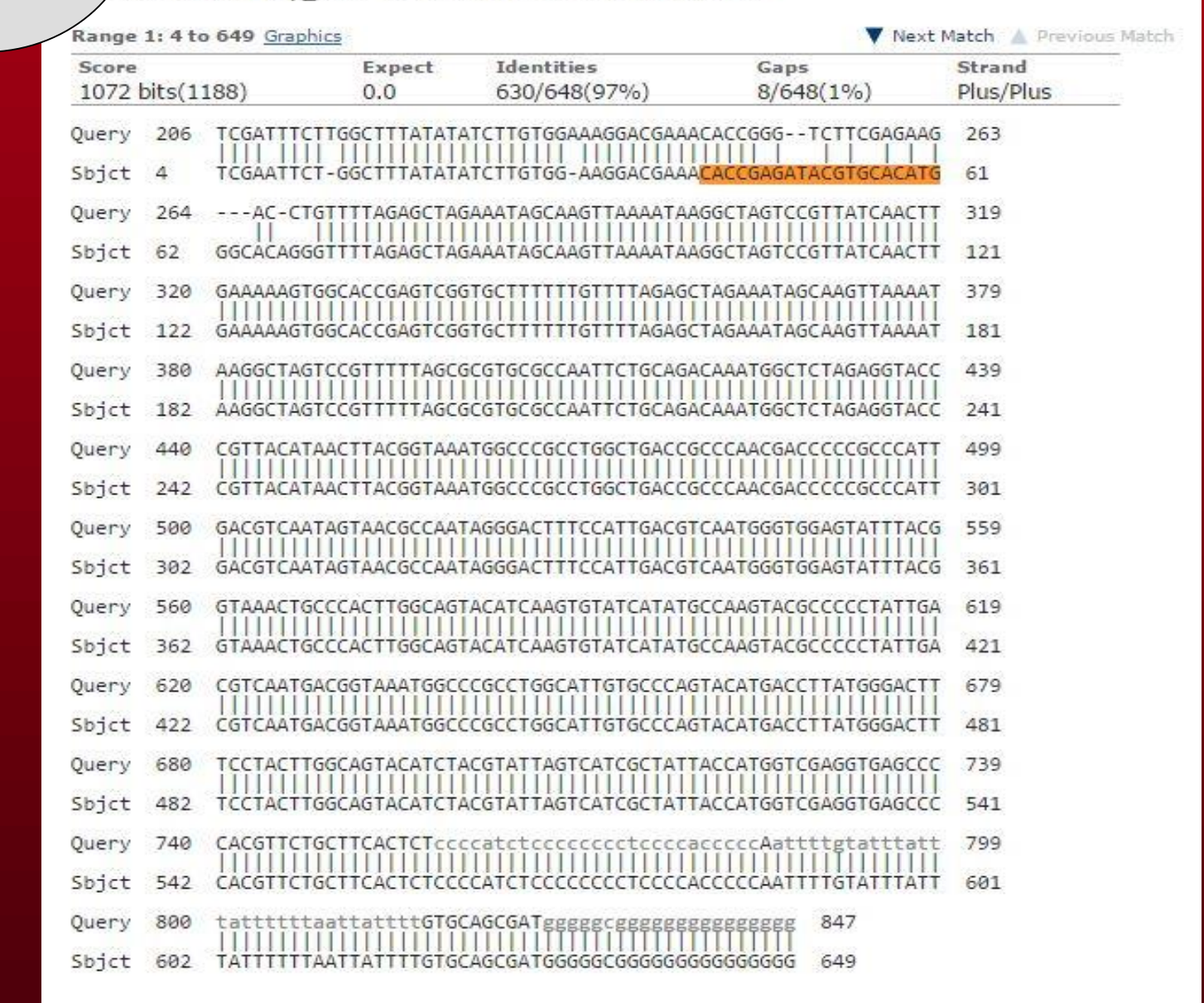
3

Purchased Oligonucleotide	Purchased Oligonucleotide Sequence
A154-18-1 p1	CACCGGTACCCTGGTCATCCTC GGG
A154-18-1 p2	AAACCCCGAGGATGACCAAGCGGT GACC
A154-18-3 p1	CACCGTTTTGGAGATACGTGCACA TGG
A154-18-3 p2	AAACCCATGTGCAGTATCTCCAAAA CC
A154-18-6 p1	CACCGAGATACGTGCACATGGGCAC AGG
A154-18-6 p2	AAACCTGTGCCATGTGCAGTAT CTC

4

Sequence Name	Colony ID	Miniprep Concentration(ng/ul)	Oligo inserted correctly?
A154-18-1	1	294.6	N
A154-18-1	2	261.6	Y
A154-18-1	3	180.3	Y
A154-18-1	4	175.7	Y
A154-18-1	5	159.3	Y
A154-18-1	1	316.3	Y
A154-18-1	26	256.8	Y
A154-18-1	38	88.3	Y
A154-18-1	16	172.5	Y
A154-18-1	24	190.8	Y
A154-18-3	1	266.7	Y
A154-18-3	2	298.1	Y
A154-18-3	1	260.5	Y
A154-18-3	3	265.2	Y
A154-18-3	4	278.3	Y
A154-18-6	1	337.8	Y

5 

6 

1. A map of the plasmid ordered from Addgene. After cloning, plasmids will contain sequences for gRNAs to target Cas9 nuclease to rat A74-UL-SNV-18. 2. A figure of how the gRNAs were selected and scored. Sequences 1, 3 and 6 were chosen. 3. A chart of the purchased oligonucleotide pairs and the corresponding sequences. These were inserted into the plasmid, and the first sequence in each pair was used to verify the sequence was inserted correctly.

Discussion

The gRNA sequences were successfully inserted into plasmids, and those plasmids were transformed into a bacteria. Approximately 94% of the oligonucleotides were inserted correctly as seen in figure 4. There was one oligonucleotide sequence that did not insert correctly. This sequence should read 5' CAC CGG TCA CGG CTT GGT CAT CCT CGG G 3', but instead it reads CAC CGG TCA CGG CTT GGT CAT CCT CCT C G 3'. This could be because the result of a mutation caused during bacterial replication. This also could be because of the way the plasmid inserted.

Future Directions

- Transiently transfect CRISPR gRNA sequence containing plasmids into rat mammary epithelial cells to target A74-UL-SNV-18.
- Compare *Mcs1b* gene transcript levels between gene-edited and unedited cell lines.

Acknowledgements

This work was supported by National Cancer Institute grant R25-CA134283, and a grant from the University of Louisville Health Sciences Research Office.

The Effects of Ligand Treatment on the Dimerization of EGFR-GFP and ErbB3-dsRED in Chinese Hamster Ovary Cells



Hailey Griffey¹, Jamie S. Rush², Brian P. Ceresa²

¹R25 Cancer Education Program, University of Louisville
²Department of Pharmacology and Toxicology, University of Louisville

Abstract

Purpose. To better understand the effects of homo- and heterodimerization between two ErbB receptor kinase family members, epidermal growth factor receptor (EGFR) and ErbB3, on the biological function of the cell.

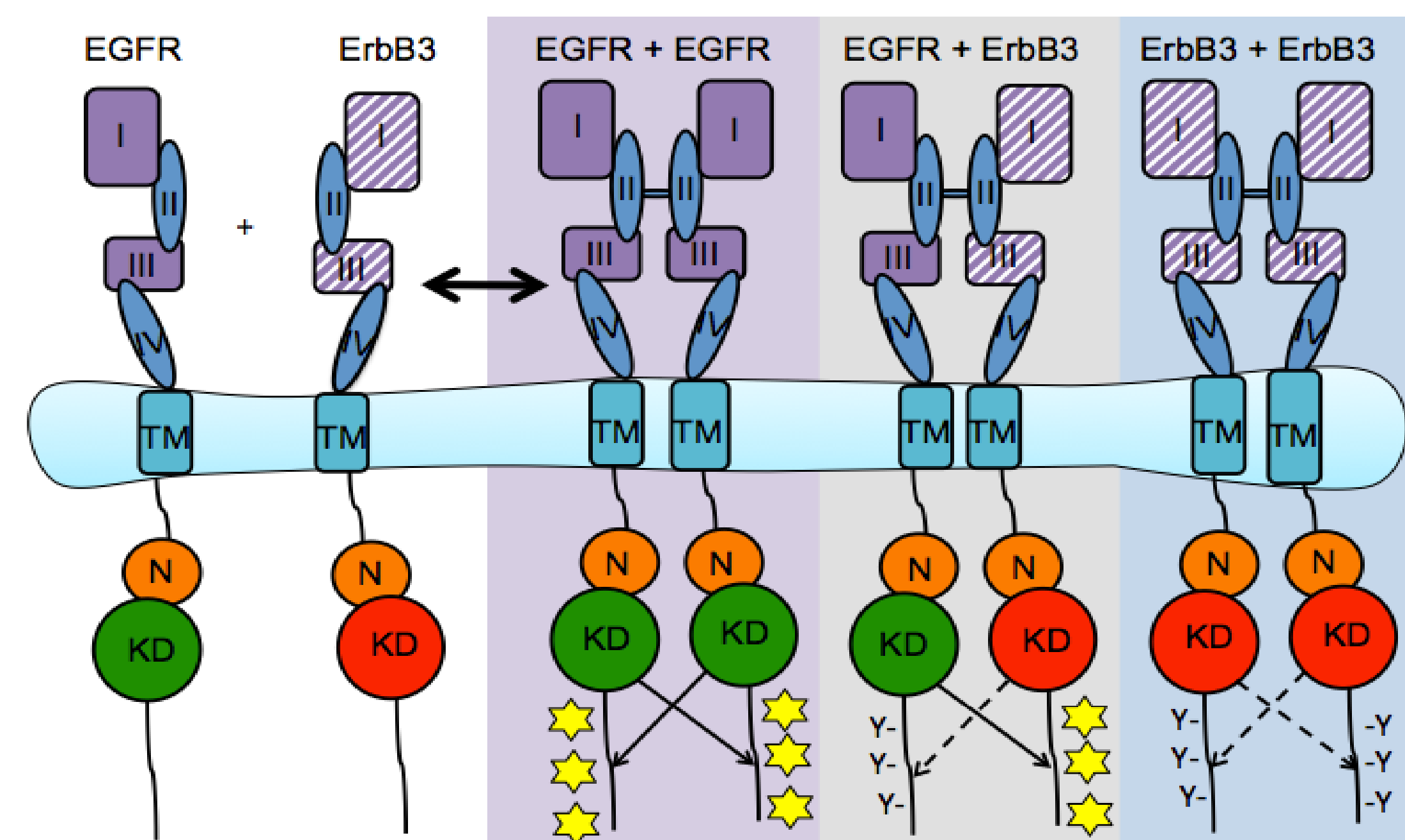
Methods. Chinese hamster ovary (CHO) cells stably and transiently express EGFR fused with a green fluorescent protein (GFP), and Erb3 fused with a red fluorescent protein (dsRED). CHO cells were serum starved and underwent dose-response using three separate ligands – EGF, BTC, and NRG1. Immunoblotting and widefield fluorescent imaging observed the presence and activity of EGFR-GFP and ErbB3-dsRED in CHO cells.

Results. Immunoblotting and widefield fluorescent imaging of transfected CHO cells demonstrate that EGFR-GFP and ErbB3-dsRED are stably present in separate clone CHO cells after transfection. Immunoblotting of phosphorylated EGFR suggests that concentrations of 4.8nM and 16nM of ligand result in significantly increased activity of the receptor kinase. Furthermore, widefield fluorescent imaging of CHO EGFR-GFP cells shows EGFR-GFP colocalized into endosomes after EGF and BTC treatments.

Conclusions. EGFR-GFP and ErbB3-dsRED are stably present in CHO cells. EGF and BTC treatment at concentrations of 4.8nM and higher promotes an increase in phosphorylation activity of EGFR-GFP. ErbB3-dsRED demonstrates little to no phosphorylation activity under ligand treatment when no other ErbB family dimer partner is present in the cell.

Background

- Lung cancer kills more Kentuckians every year than the next eight most common cancers combined (www.kentuckyonehealth.org)
- About 85% to 90% of lung cancers are non-small cell lung cancer (www.cancer.org)
- Non-small cell lung cancer is associated with a mutation in the epithelial growth factor receptor (EGFR) (Paez et al., *Science*)
- Increased expression levels of ErbB3 have been linked to a higher risk of metastasis development in non-small cell lung cancer (Müller-Tidow et al., *Cancer Research*)



ErbB receptor tyrosine kinases are a four-membered family that exhibit the same basic structure: an extracellular domain, an intracellular domain, and a transmembrane section. The extracellular portion has two ligand-binding domains and two cysteine-rich domains (I-IV). Once a ligand binds to this region, it activates the kinase domain located in the intracellular portion and causes the receptor kinase to form dimers with other ErbB family members. The activated kinase domain trans-phosphorylates the tyrosine residues of its dimer partner.

Although similar in structure, EGFR and ErbB3 demonstrate key differences in kinase domain activity and ligand-binding domains. EGFR has a functional kinase domain and can phosphorylate the tyrosine residues of its dimer partner. ErbB3, however, has diminished kinase activity. This results in less phosphorylation to its partner, and therefore less docking sites to create a signaling cascade that elicits a cellular response. The homo- or heterodimerization between ErbB3 family members ultimately determines which tyrosine residues are phosphorylated, and therefore which effectors interact with the receptor. If EGFR can heterodimerize with ErbB3, most phosphotyrosines will be present on the ErbB3 receptor. ErbB3 has been shown to be an important contributor to migration response in cells. We hypothesize that the EGFR:ErbB3 complex will result in an interaction with effectors that promote cellular migration, which could be linked to the development of metastasis in carcinoma cells.

Hypothesis

EGFR and ErbB3 heterodimerization could potentially contribute to the aggression and metastasis expressed in cancer cells

Questions

Can EGFR-GFP and ErbB3-dsRED be stably expressed in CHO cells?
 Can ligand treatment activate CHO EGFR-GFP and CHO ErbB3-dsRED cells?
 Is there ligand specific redistribution of EGFR-GFP and ErbB3-dsRED in CHO cells?

Figure 1

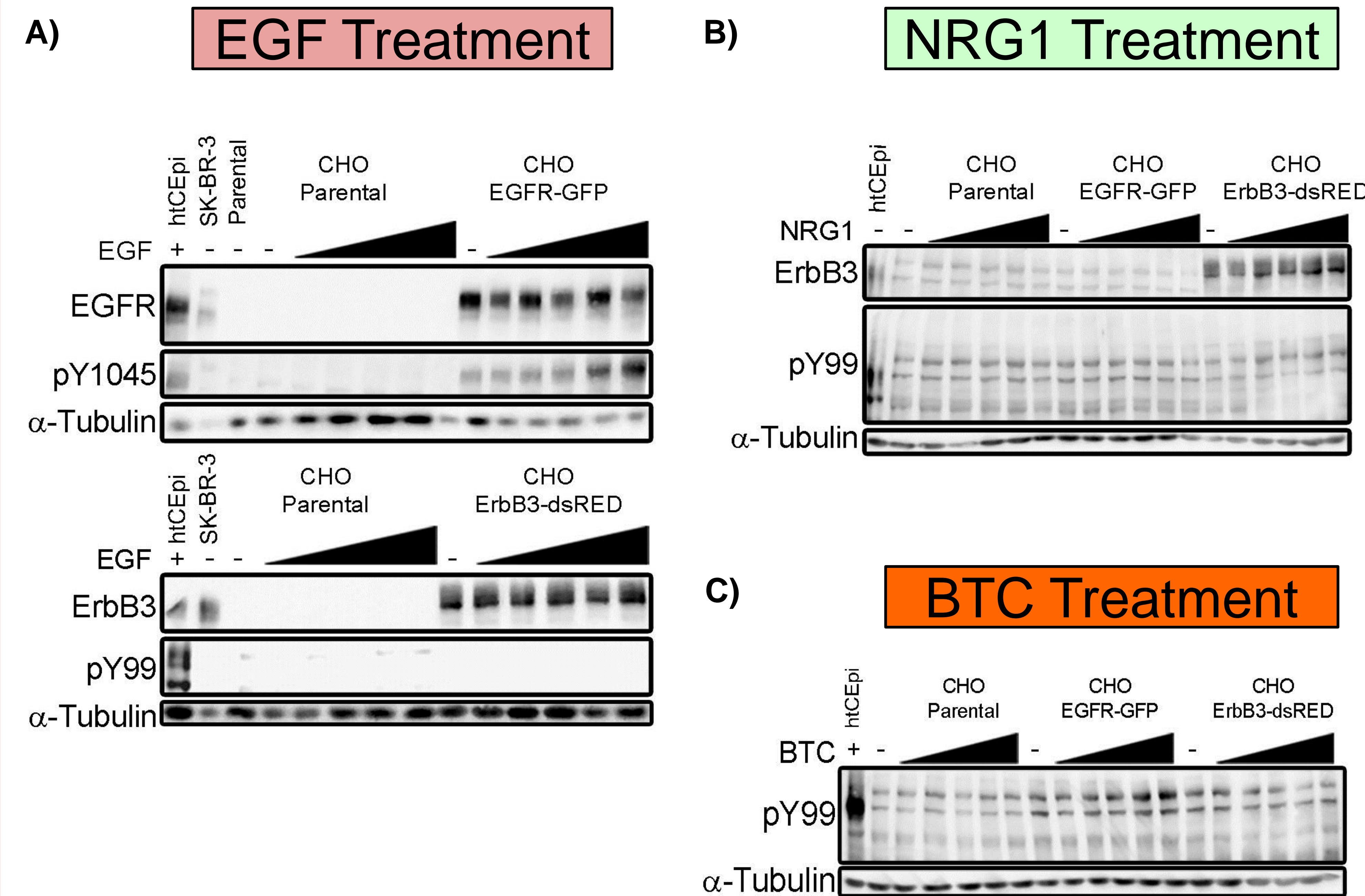


Figure 1. The effects of increasing concentrations of EGF, NRG1, and BTC on CHO cells Stable cell lines were generated using plasmids encoding for either EGFR-GFP or ErbB3-dsRED and selected in the presence of 800 μg/mL G418. Single cell colonies were then created by FACS, eliminating all non-fluorescing cells. For panels A, B, and C, cells were serum-starved for two hours at 37°C in 5% CO₂ and then treated with EGF, BTC, or NRG1 at concentrations of 0nM, 0.16nM, 0.48nM, 1.6nM, 4.8nM, 16nM. Cells were then harvested and equal amounts of protein loaded and resolved through SDS-PAGE. The gel was then transferred to a nitrocellulose membrane and treated with various antibodies. **A)** EGF treated cells were analyzed using Western blot assay. htCEpi cells are used as a positive control for total EGFR and phosphorylated EGFR, SK-BR-3 is used as a positive control for ErbB3, and α-tubulin is a gel loading control. The membrane was then probed for total EGFR, total ErbB3, a specific phosphotyrosine (pY1045), and α-tubulin. **B)** All CHO cell lines were treated with NRG1. Parental CHO cells are a negative control, htCEpi cells are a positive control, and α-tubulin is a loading control. Membrane was probed for total ErbB3, all phosphotyrosines (pY99), and α-tubulin. **C)** BTC treated CHO cell lines were probed for pY99 and α-tubulin. All treatments n = 2-3

Figure 2

Figure 2. Widefield fluorescent imaging of EGFR-GFP, ErbB3-dsRED, Parental, EGFR-GFP/ErbB3-dsRED CHO ErbB3-dsRED cells were transiently transfected with EGFR-GFP using Lipofectamine 2000 and then incubated overnight at 37°C. CHO cell lines were serum-starved for two hours at 37°C, and treated with 16nM EGF, NRG1, or BTC for fifteen minutes. Coverslips were then fixed with 4% paraformaldehyde. Coverslips were mounted to slides using prolong with DAPI, and then imaged using widefield fluorescent imaging. Scale bar represents 10μm. n = 2

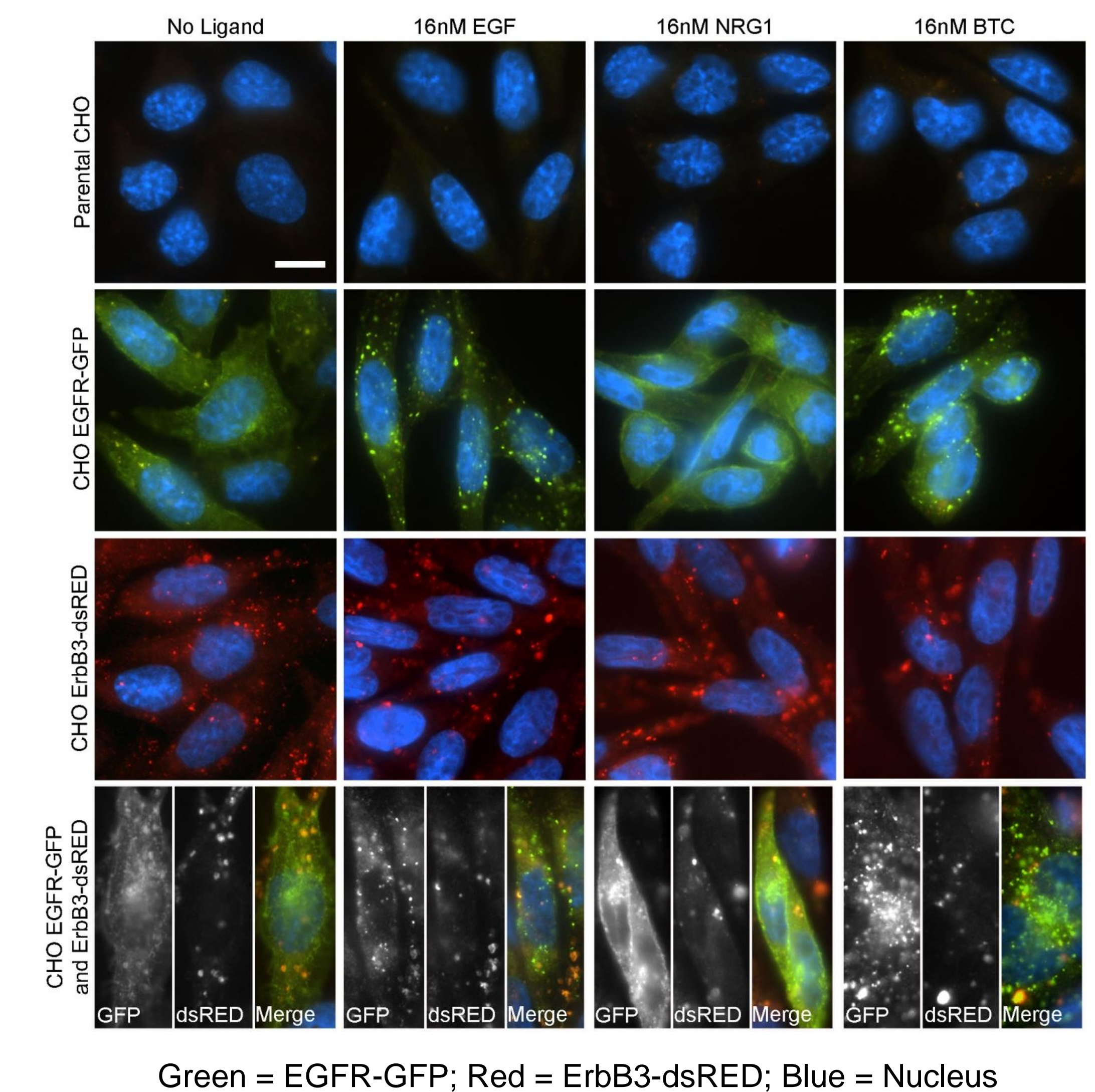


Figure 3

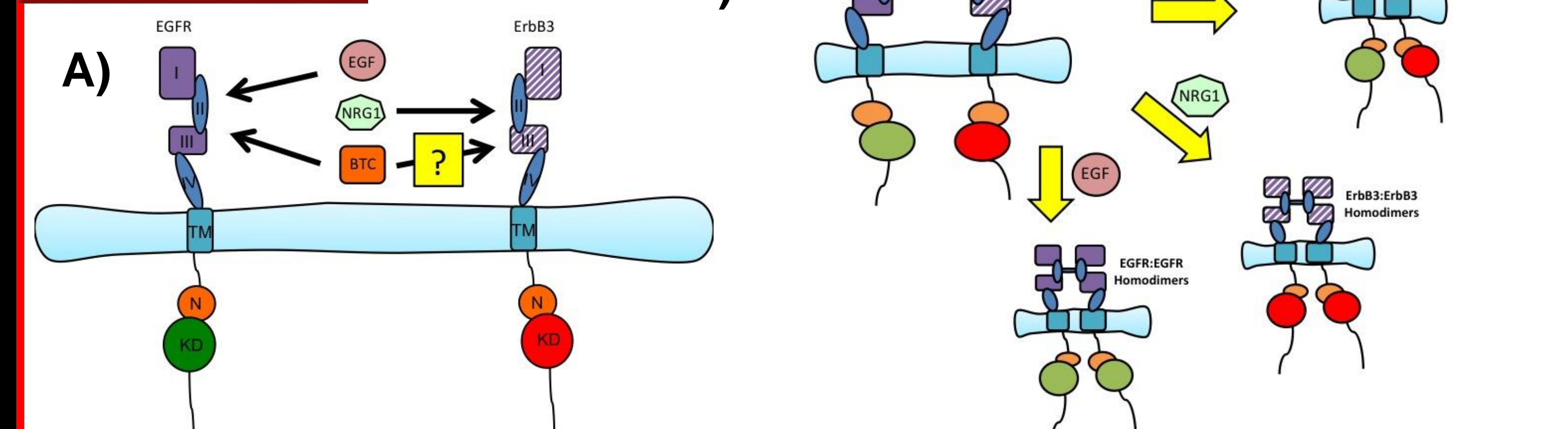


Figure 3. Schematic of the hypothetical relationship between EGFR and ErbB3 under ligand treatment **A)** EGFR has been known to bind EGF and BTC; ErbB3 has been known to bind NRG1 (Hynes and MacDonald, *ScienceDirect*). Whether BTC can bind to ErbB3 is unknown. **B)** It is hypothesized that EGF treatment will induce primarily EGFR homodimers, NRG1 treatment will produce ErbB3 homodimers, and BTC treatment will result in the heterodimerization of EGFR and ErbB3.

Conclusion

Chinese Hamster Ovary cells express stably transfected EGFR-GFP and ErbB3-dsRED in separate clone cell lines. EGFR-GFP is capable of being activated after treatment of ligands EGF and BTC in CHO EGFR-GFP cells, particularly at concentrations of 4.8nM and higher. Ligand treatment appears to have little to no effect on the activity of ErbB3-dsRED in CHO ErbB3-dsRED cells, most likely due to diminished kinase activity of ErbB3. Furthermore, EGF and BTC treatment to CHO cells containing EGFR-GFP and transiently transfected CHO cells containing both EGFR-GFP and ErbB3-dsRED demonstrate minimal colocalization and compartmentalization of receptor.

Future directions: Create a stably dual-transfected CHO cell lines containing varying levels of both EGFR-GFP and ErbB3-dsRED in order to determine how receptor density affects heterodimerization formation between these receptor kinases. Induce heterodimerization between EGFR-GFP and ErbB3-dsRED and observe how this effects the proliferation/migration of the cell.

Acknowledgements

R25 Cancer Education Program, Ceresa Lab Members
 Funding: NCI R25-CA134283

Design and Synthesis of Polymer Blend Electrospun Fibers for Sustained Release of siRNA to the Female Reproductive Tract

Justin S. Heidel¹, Jill M. Steinbach¹

Department of Bioengineering¹

University of Louisville, J. B. Speed School of Engineering

Introduction

Efficacious preventative and therapeutic agent delivery to the female reproductive tract (FRT) is challenging due to the harsh microenvironment of the FRT, causing rapid degradation and clearance – especially of biological agents including genes and proteins. To overcome these challenges, nanotechnologies, such as electrospun fibers (EFs), can be customized and utilized for encapsulation, specific targeting, and sustained delivery of biologics and chemotherapeutics. Factors including surface morphology and fiber diameter can be altered, enabling high encapsulation, prolonged release, and subsequently efficacious biodistribution. Due to this versatility, nanofibers prove to be an exciting and promising platform for gene and drug delivery to the FRT. **The immediate goal of this study was to engineer poly(lactic-co-glycolic acid)-poly(ethylene oxide) (PLGA-PEO) and poly(DL-lactone-co-ε-caprolactone)-poly(ethylene oxide) (PLCL-PEO) blend fibers to achieve high encapsulation efficiency and sustained release of siRNA.** Here we evaluated EF morphology, size, loading, and controlled-release to obtain a better understanding of the factors that modulate EF properties and delivery to the FRT. **The long-term goal of this study is to evaluate the most promising formulation of the above EFs to deliver siRNA targeting the HPV18 E6 oncogene in HeLa cells *in vitro*.** We hypothesize that these siRNA EFs will provide an efficacious delivery platform to initially protect and sustainably deliver siRNA in the unique microenvironment of the FRT. Here we provide a preliminary assessment of the novel EFs to encapsulate and release siRNA from our polymer blended and non-blended EF formulations. The results of this study will allow us to rationally design formulation(s) to provide the most effective siRNA delivery to decrease expression of our desired target E6 oncogene in future studies.

Methods

EF Formulations: In this study, we designed and synthesized the following EF formulations:

PLGA (50:50 Lactic Acid:Glycolic Acid)

100% PLGA
90:10 PLGA:PEO
75:25 PLGA:PEO

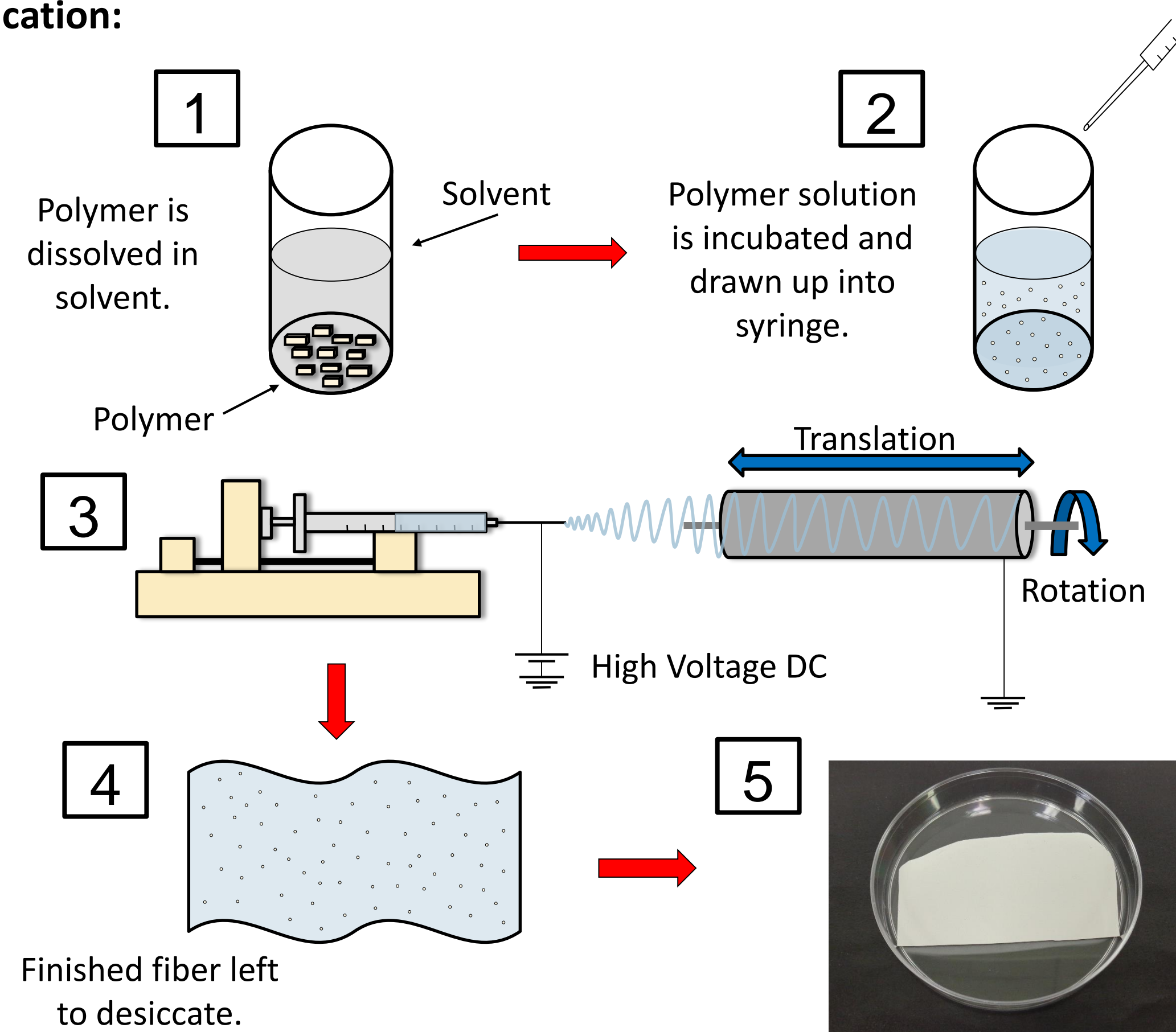
PLCL (80:20 Lactone:Caprolactone)

100% PLCL
90:10 PLCL:PEO
75:25 PLCL:PEO

Encapsulant: siMimic oligonucleotide sense and antisense strands were annealed and complexed with spermidine prior to electrospinning.

5'-GTGTCAAGTCCAATCTATG-3'
3'-CACAGTTCAGGTTAGATAC-5'

EF Fabrication:



EF Characterization: We performed scanning electron microscopy (SEM) to evaluate EF surface morphology and size. We used PicoGreen to measure the amount of siMimic we encapsulated in our EFs. To determine the amount of siMimic released from our EFs, we evaluated controlled release in both phosphate-buffered saline (PBS) and simulated vaginal fluid (SVF).

Results

Effect of Polymer Percent on EF Diameter and Morphology

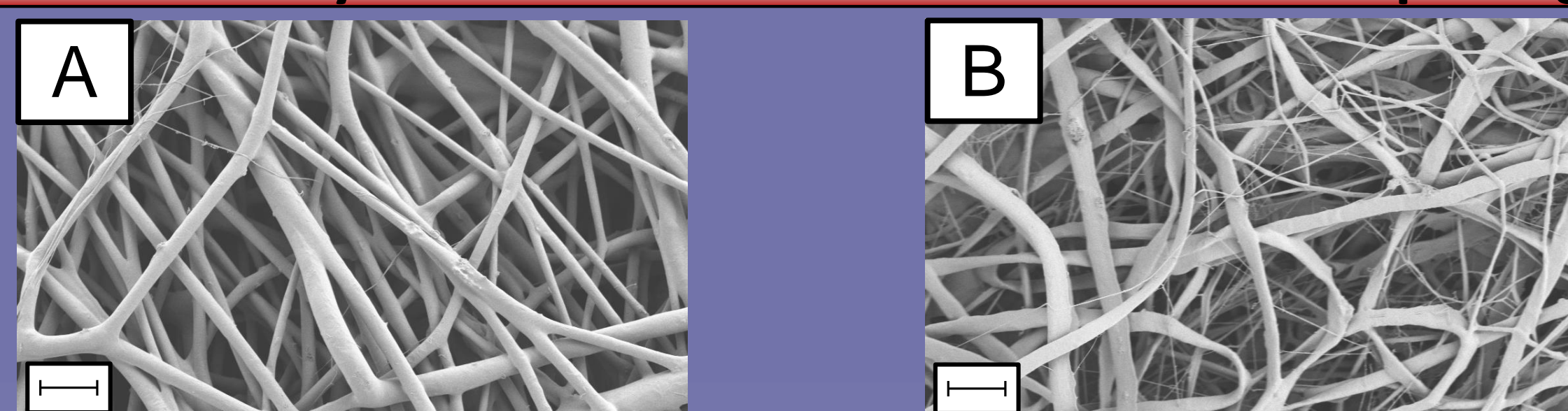


Figure 1. SEM images of: (A) 15% PLGA-PEO and (B) 9% PLGA-PEO. Scale bar = 10 μm.

Effect of Solvent on Polymer Blend Formulation

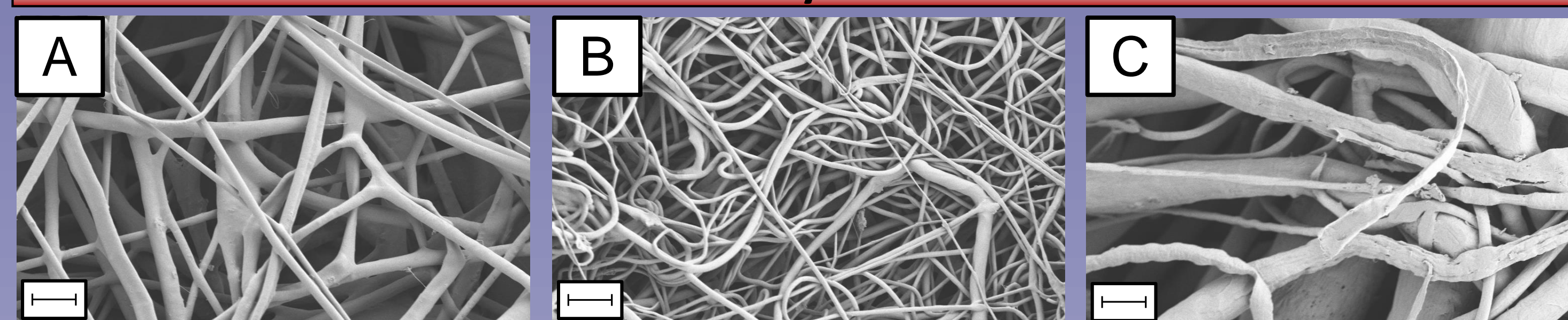


Figure 2. SEM images of: (A) PLGA-PEO in HFIP, (B) PLGA-PEO in DCM 4:1 DMF, and (C) PLGA-PEO EFs in HFIP 4:3 Water. Scale bar = 10 μm.

siMimic Encapsulated EFs

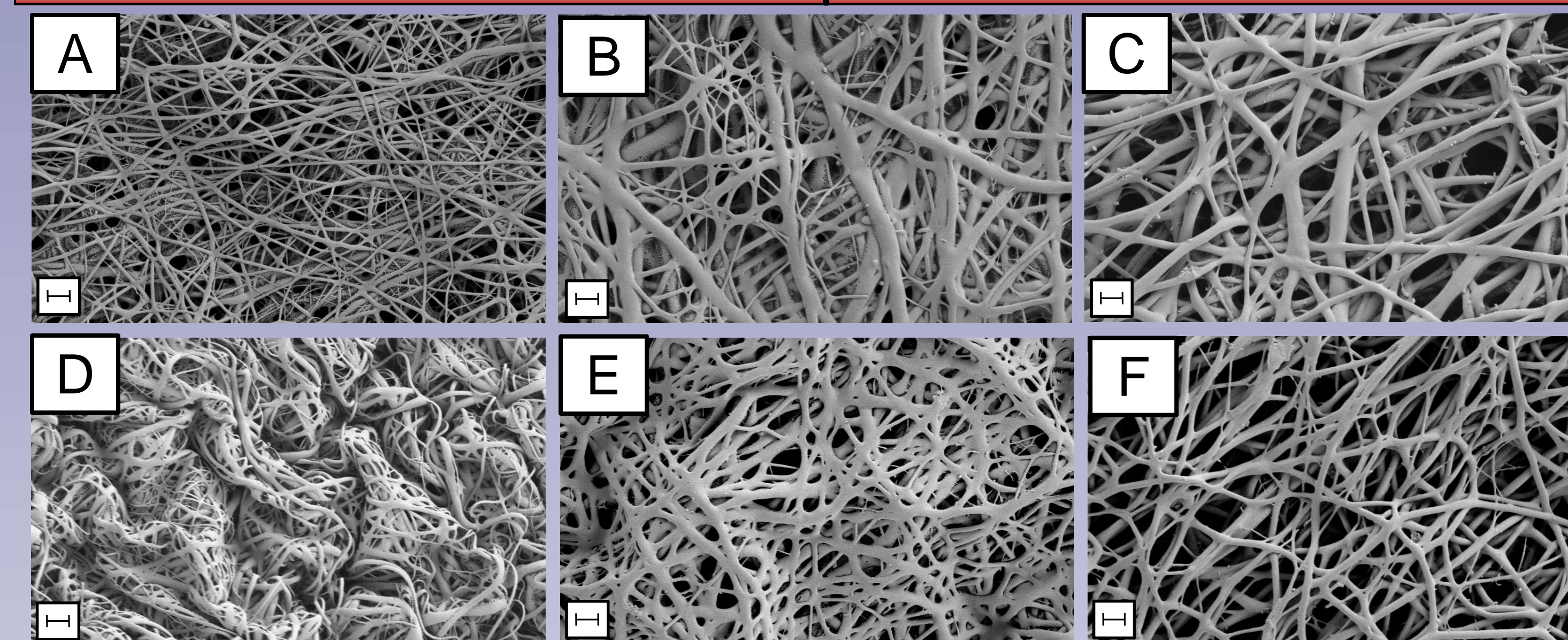
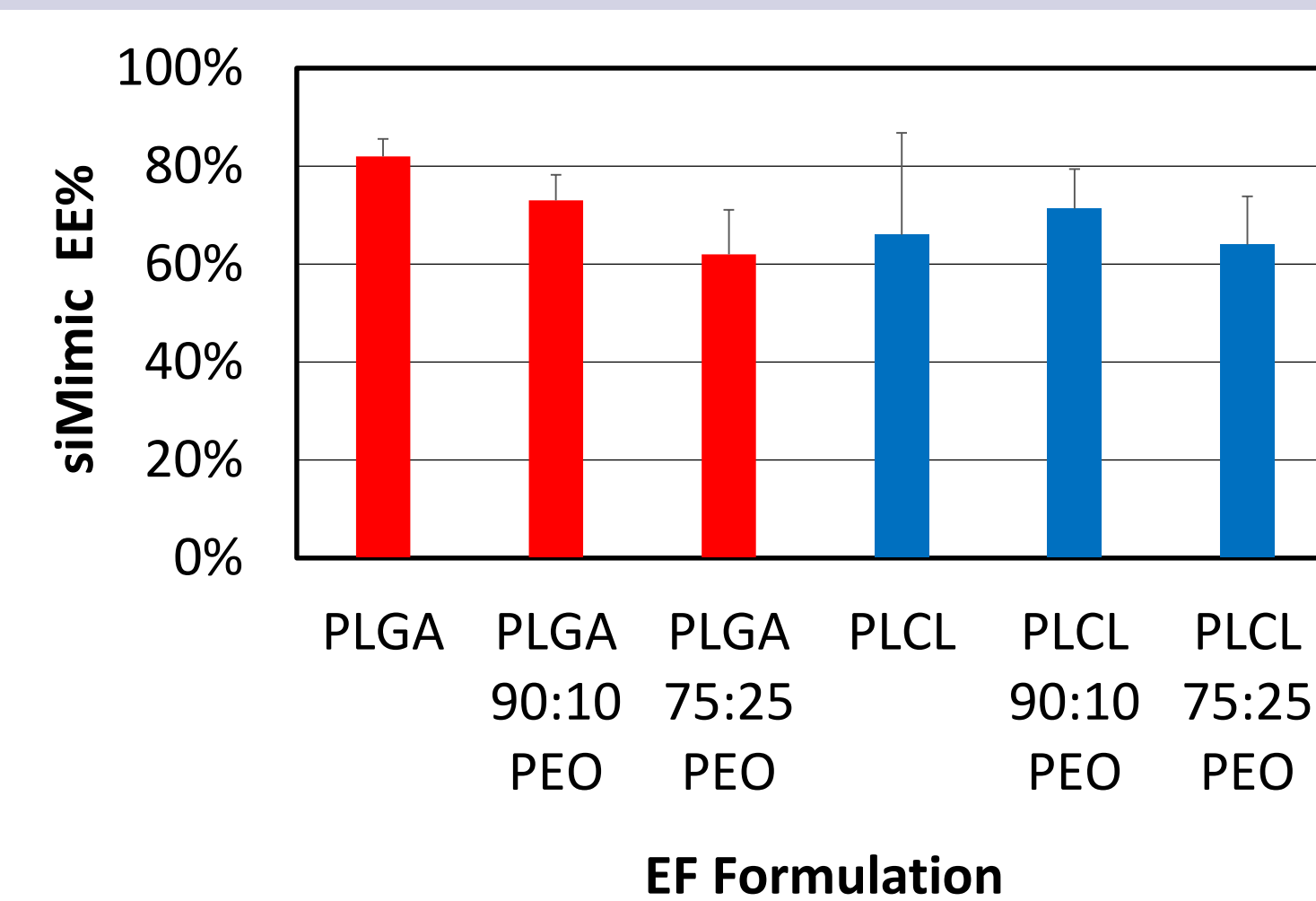


Figure 3. SEM images of: (A) PLGA, (B) PLGA 90:10 PEO, (C) PLGA 75:25 PEO, (D) PLCL, (E) PLCL 90:10 PEO, (F) PLCL 75:25 PEO EFs with siMimic and spermidine. Scale bar = 1 μm.

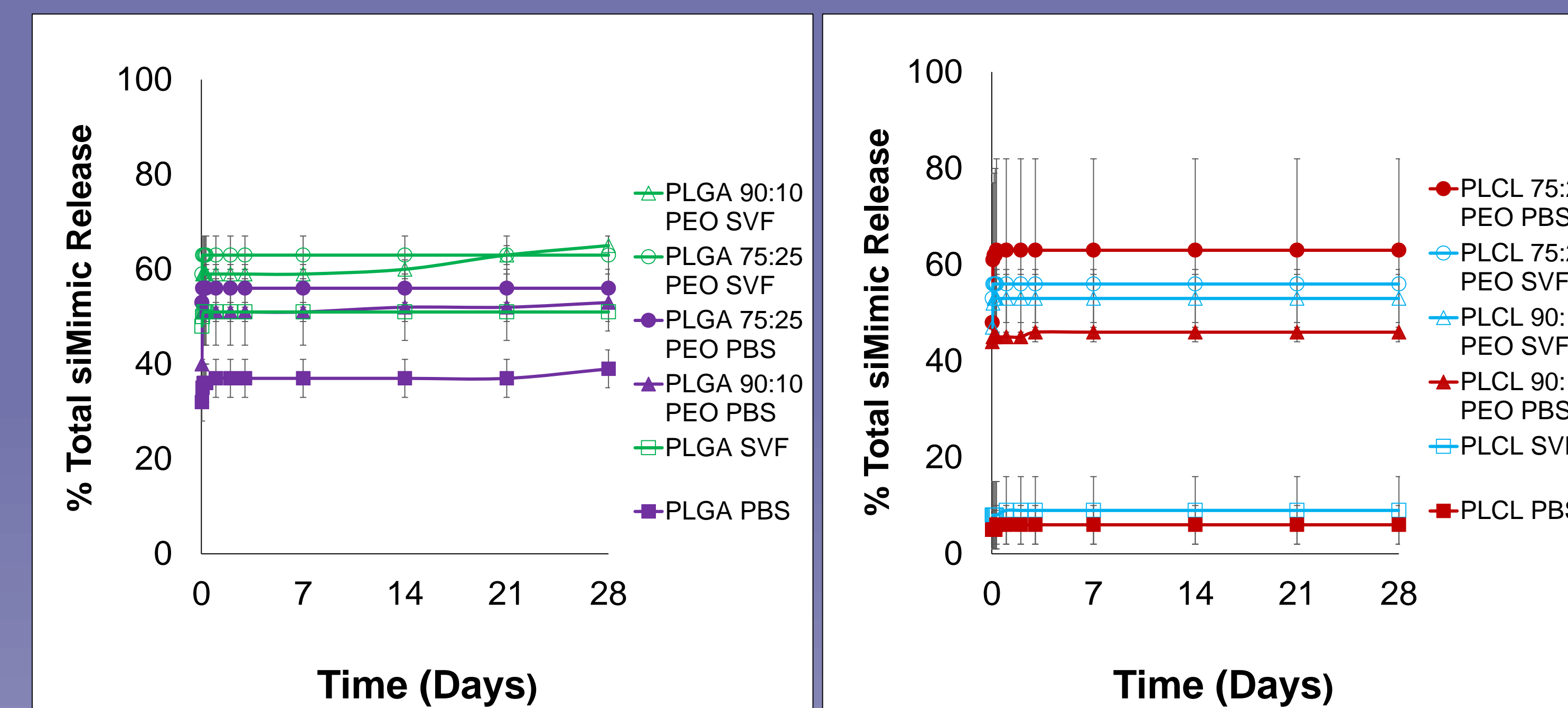
siMimic Loading



Formulation	Loading (pmol/mg polymer)	EE
PLGA	816±36	82±4%
PLGA 90:10 PEO	726±53	73±5%
PLGA 75:25 PEO	618±91	62±9%
PLCL	660±208	66±21%
PLCL 90:10 PEO	713±81	71±8%
PLCL 75:25 PEO	637±98	64±10%

Figure 4 & Table 1. Loading and encapsulation efficiency (EE) of siMimic in EFs.

Controlled Release



EF Formulation	Maximum Release in PBS (pmol/mg)	Maximum Release in SVF (pmol/mg)
PLGA	310	415
PLGA 90:10 PEO	385	468
PLGA 75:25 PEO	347	391
PLCL	40	57
PLCL 90:10 PEO	356	376
PLCL 75:25 PEO	401	325

Figure 5 & Table 2. Controlled release of siMimic from EFs in phosphate-buffered saline (PBS) and simulated vaginal fluid (SVF).

Future Studies

- Apply EF polymer blend formulations to synthesize and fully characterize actual siRNA EFs.
- Examine the efficacy of the "optimal" EF platform to distribute siRNA to HeLa cell monolayers (2-D) and tumor spheroids (3-D).
- Determine the efficacy of E6 siRNA EFs on mRNA expression in HeLa monolayers and spheroids.

Conclusions

- All EF formulations displayed well-delineated morphology and high encapsulation efficiencies (> 60%, greater than that of nanoparticles, which have an EE of ~30-40%).
- PLGA 90:10 PEO EFs displayed the most release of siMimic and appear to be the most promising for future gene delivery.
- Incorporation of PEO significantly enhances release for PLCL EFs, while having less effect on PLGA EFs.

Acknowledgements

This research is supported by the University of Louisville Cancer Education Program NCI R25-CA134283. Thank you, Dr. Stuart Williams for allowing us to use your electrospinning apparatus.



Perceived survivorship needs in patients with human papillomavirus (HPV)-positive and (HPV)-negative head and neck cancer

Erica G. Holland¹, Rebecca A. Redman, M.D.^{2,3}

University of Louisville

School of Nursing¹, School of Medicine Division of Medical Oncology², James Graham Brown Cancer Center³

Introduction

As the survivorship rates for cancer patients increase, the need for survivorship resources is also increasing. The demographics of head and neck cancer are changing with the emerging role of HPV-induced cancers. Patients diagnosed with HPV-positive oropharyngeal cancers are, on average, 10 years younger than patients with tobacco and/or alcohol-induced cancers. In addition, men with HPV-induced tumors outnumber women 3:1.

We hypothesize that the survivorship needs of patients with HPV-positive tumors will differ significantly from those with tumors induced by smoking and/or alcohol.

Methods

For this study, patients were asked to partake in a survey. We included patients with squamous cell carcinoma of a mucosal site of the head and neck treated with curative intent. Patients with other histologies and those treated with palliative intent were excluded. Collected data included demographics (age, gender, race, income level, cancer site, stage, tobacco and alcohol history), and planned or completed treatment regimens. Patients were asked about which phase of treatment they were in (haven't started, in the midst, completed/how long ago?), and then to rank their concerns after treatment in order of importance to them. They were also asked about various resources, and how useful they felt those resources would be.

Results

A total of 20 surveys have been distributed and returned thus far. Of those completed, 40% were patients with HPV+ head and neck cancer. Regardless of HPV status, the most commonly cited survivorship concerns were physical side effects, followed by cancer recurrence, cosmetic side effects, and emotional side effects.

With regard to survivorship resource utilization, 50% of patients reported or anticipated pain after completion of treatment. In addition to pain management, patients also reported an interest in nutritional counseling, support groups, and complementary/alternative therapies. In this small sample size, this did not differ between patients with HPV+ and patients with HPV- tumors.

Figure 2: Survivorship resources patients reported they were most likely to use

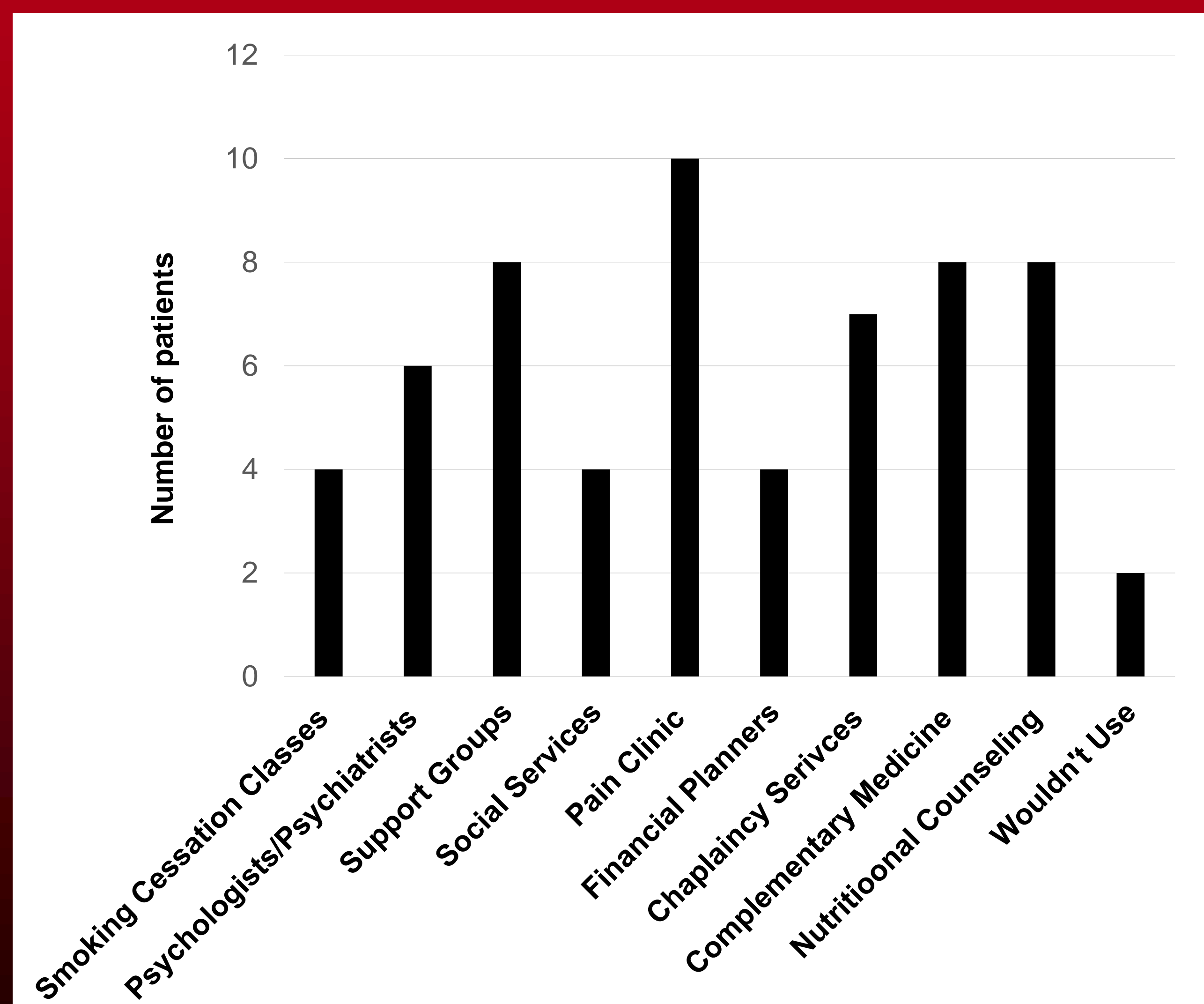


Figure 1: Patient-reported concerns after treatment

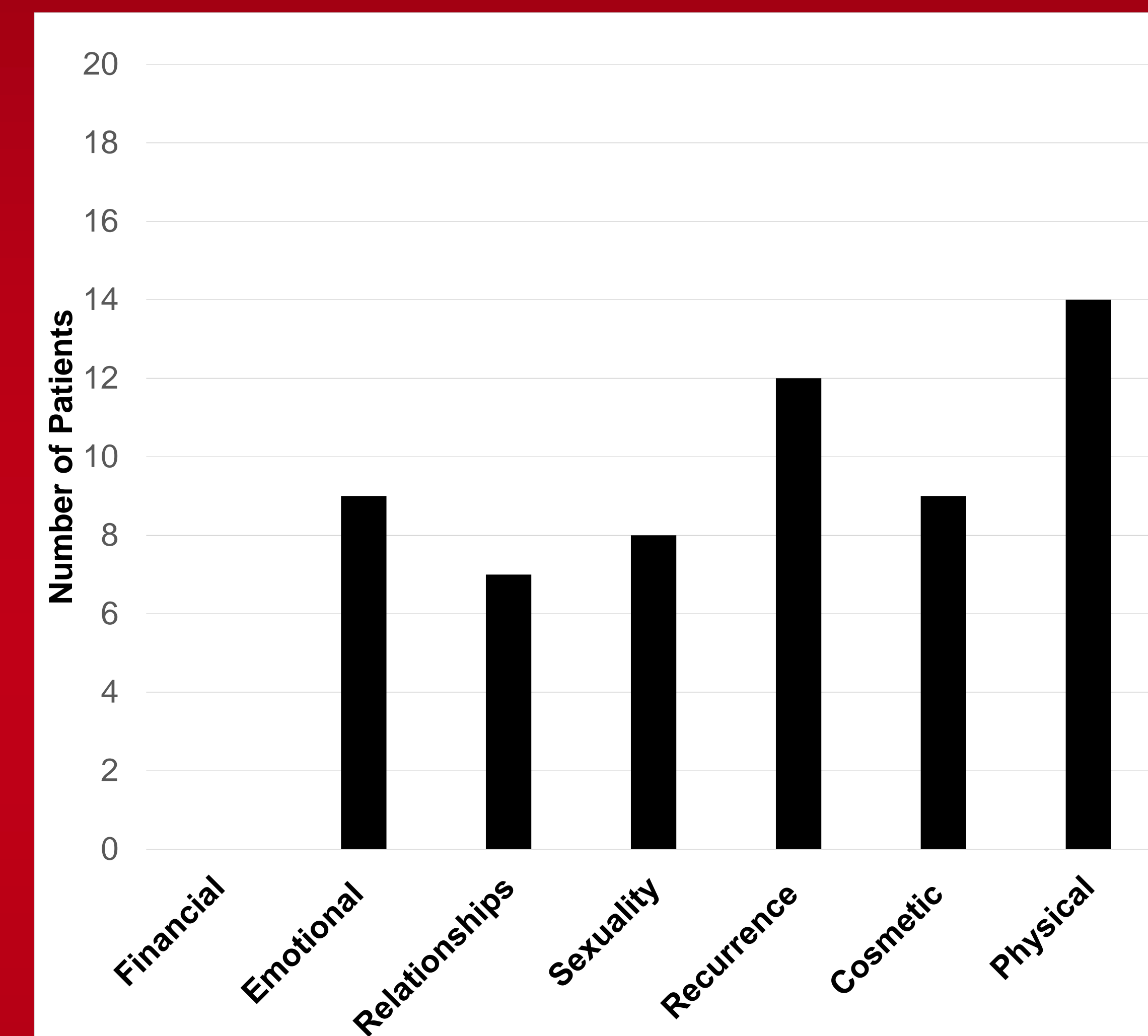


Table 1: Patient demographics

Variable		Patients (n, %)
HPV	Positive	8, 40%
	Negative	12, 60%
Gender	Male	14, 70%
	Female	6, 30%
Cancer Site*	Tongue	8, 40%
	Tonsil	4, 20%
	Neck	5, 25%
	Larynx	1, 5%
	Unknown	2, 10%
Age Range	20-40	1, 5%
	41-55	6, 30%
	56-70	9, 45%
	71-85	4, 20%

*Cancer site is reported as listed by the patient. Neck is a site of regional metastasis.

Conclusions

In this preliminary analysis, physical side effects of treatment and risk of cancer recurrence dominate survivorship concerns of patients with head and neck cancer, regardless of tumor HPV status. Of various survivorship resources available, patients reported they were most likely to use pain management services, support groups, complementary medicine, and nutritional counseling. Only 10% of patients surveyed reported that they would not utilize any of these resources. Data collection and survey administration are still ongoing.

Acknowledgements

Research supported by a grant from National Cancer Institute grant R25-CA134283 and the School of Medicine Summer Research Scholar Program.

Mechanistic Insight Into Vinyl Chloride-Induced Liver Injury: Role of Dietary Fatty Acids.

Brenna Kaelin¹, Adrienne M Bushau¹, Lianne C Anders¹, Heegook Yeo¹, Gavin E Arteel¹, Matt Cave^{1,2,3}, Craig J McClain^{1,2,3} and Juliane I Beier¹

Departments of ¹Pharmacology and Toxicology, and ²Medicine; University of Louisville Health Sciences Center, Louisville, KY 40292, and the ³Robley Rex Louisville VAMC, Louisville, KY 40206, USA.

Abstract

Background. Vinyl chloride (VC) is a relevant chemical toxicant and an important occupational/environmental pollutant. Most studies on the risk of VC exposure to human health have focused on the effect of VC alone (high doses) and not taken into consideration VC interactions (low doses) with risk-modifying factors. It has been shown that certain types of dietary fat such as polyunsaturated fatty acids (PUFA), linoleic acid (LA) in particular, exacerbate fatty liver diseases. Bioactive oxidized linoleic acid metabolites (OXLAMs) play a critical role in the development/progression of hepatic inflammation and injury in the context of steatosis. We hypothesize that VC exposure may synergize hepatic damage caused by NAFLD by increasing production of OXLAMs. The purpose of the current study was to determine the role of LA metabolites in sensitizing the liver to VC via molecular, organelle, and cellular effects.

Methods. Mice were administered a bolus dose of chloroethanol (or vehicle) 10 wks after being fed a linoleic acid rich high fat diet (HPUFA; 42% corn oil)-fed or low fat control diet (LPUFA; 13% corn oil). Animals were sacrificed 0-24 hours after ClEtOH exposure. Samples were harvested for determination of liver damage, inflammation, oxidative and ER stress.

Results. In LFD-fed control mice, chloroethanol caused no detectable liver damage or inflammation. In HPUFA-fed mice, chloroethanol increased HPUFA-induced liver damage, steatosis, infiltrating inflammatory cells and hepatic expression of proinflammatory cytokines and genes affected in ER stress. Furthermore, chloroethanol altered protein expression of key genes involved in ER stress.

Conclusions. Taken together, VC and HPUFA cause liver damage, inflammation and ER stress markers. This serves as proof-of-concept that VC hepatotoxicity may be modified by a linoleic acid rich diet. These data implicate exposure to VC as a risk factor in the development of liver disease in susceptible populations.

BACKGROUND

Over 33% of US adults are obese (BMI ≥ 30) with another 34.2% being overweight (BMI ≥ 25).¹ One of the major health effects of obesity is non-alcoholic fatty liver disease (NAFLD). Indeed, the burden of liver disease has increased in the US in parallel with the obesity epidemic.² However, it is assumed that there are other contributing factors (e.g., environmental factors) that determine overall risk for developing the disease.

Vinyl chloride is found in significant concentrations in the ambient air and the ground water surrounding manufacturing complexes. Therefore, exposure to VC is widespread in industrialized nations. Historically VC-exposure has been associated with hemangiosarcoma, HCC and fibrosis. The Louisville industrial area ('Rubbertown') is a well documented site for VC-induced liver diseases.³ What is unknown is what low level (sub-NOAEL) exposure will do to the risk of underlying liver diseases. While it is clear that high doses of VC are directly hepatotoxic to humans, the effects of lower doses of VC and its interactions with overnutrition on overall liver health have not been determined.

The risk for developing fatty liver disease is not based solely on one factor, but rather is modified by other mitigating conditions, such as genetic (e.g., polymorphisms in key genes) or environmental (e.g., diet, lifestyle, etc) factors. Numerous studies have now established that physiological/biochemical changes to liver that are pathologically inert can become hepatotoxic in response to a second agent. This '2-hit' paradigm has been best exemplified in non-alcoholic fatty liver diseases.⁴ We propose that low-dose VC may also serve as a second hit. The metabolism of VC is similar to that of ethanol, which also causes fatty liver disease. VC is metabolized via an CYP2E1 and aldehyde dehydrogenase dependent pathway. Indeed, a key pathologic characteristic of VC-induced TASH in humans is steatohepatitis analogous to ASH or NASH. VC-metabolites may therefore be important mediators of VC-enhanced NAFLD.

Recent work has suggested that the deelopment of 'classical liver diseases' (e.g., ASH and NASH) involve endoplasmic reticulum (ER) stress. ER stress is induced when homeostasis of synthesis, folding, and secretion of proteins is disrupted.⁵ It is not known if TASH i.e., exposure to VC and its metabolites induces ER stress.

MATERIALS AND METHODS

Animals and treatments. Eight week old male C57BL/6J mice were obtained from Jackson Laboratory (Bar Harbor, ME). Animals were administered a corn oil diet and some were injected with a dose of chloroethanol (50 mg/kg i.g.). Animals were sacrificed and blood and tissue were collected for further analyses.

Cell culture and treatments. HepG2 cells from ATCC (Manassas, VA) were exposed to (1, 2.5, 5, 10, 20 μM, 50 μM, 80 μM, and 100 μM of chloroacetaldehyde). Cells were plated at 200,000 cells per well for 12-well plate. RNA was extracted after 6 hours.

Lipid Extraction. Lipids were extracted from the livers of the treated mice. The lipids were diluted 1:10 and sonicated for the triglyceride assay. The lipids were then sonicated again for the cholesterol assay with no dilutions.

Biochemical analyses and histology. Plasma levels of ALT, AST were determined using standard kits (ThermoTrace, Melbourne, Australia). Paraffin-embedded sections of liver were stained with hematoxylin & eosin (H&E) to assess overall hepatic structure, and Periodic acid-Schiff reagent (PAS) to detect glycogen. Neutrophil accumulation in the livers was assessed by staining tissue sections for chloroacetate esterase (CAE), a specific marker for neutrophils, using the naphthol AS-D chloroacetate esterase kit (Sigma, St. Louis MO).

RNA isolation and real-time RT-PCR. Total RNA was extracted from liver tissue samples by a guanidium thiocyanate-base method (RNA STAT 60 Tel-Test). 1 μg total RNA per sample was reverse transcribed. PCR was performed using the ABI StepOne Plus. The comparative C_t method was used to determine fold differences between samples.

Immunoblots. Protein was extracted from HepG2 cells. 10 μg and 20 μg of total protein was loaded onto SDS-polyacrylamide gels followed by electrophoresis and Western blotted onto PVDF membranes. Antibodies were used at the dilutions recommended by the suppliers. Horseradish peroxidase-coupled secondary antibodies and chemiluminescence detection reagents were from Pierce (Rockford, IL, USA). The signals were detected employing Classic Blue™ autoradiography film BX (MIDSCI, St. Louis, MO). Densitometric quantitation was performed with UN-SCAN IT analysis software (Silk Scientific, Orem, UT).

Statistics. Summary data represent means ± SEM (n = 4-6). ANOVA with Bonferroni's post-hoc test or the Mann-Whitney rank sum test was used for the determination of statistical significance among treatment groups, as appropriate. *In vivo*: ^a, p < 0.05 compared to vehicle; ^b, p < 0.05 compared to animals exposed LPS alone. *In vitro*: ^a, p < 0.05 compared to vehicle.

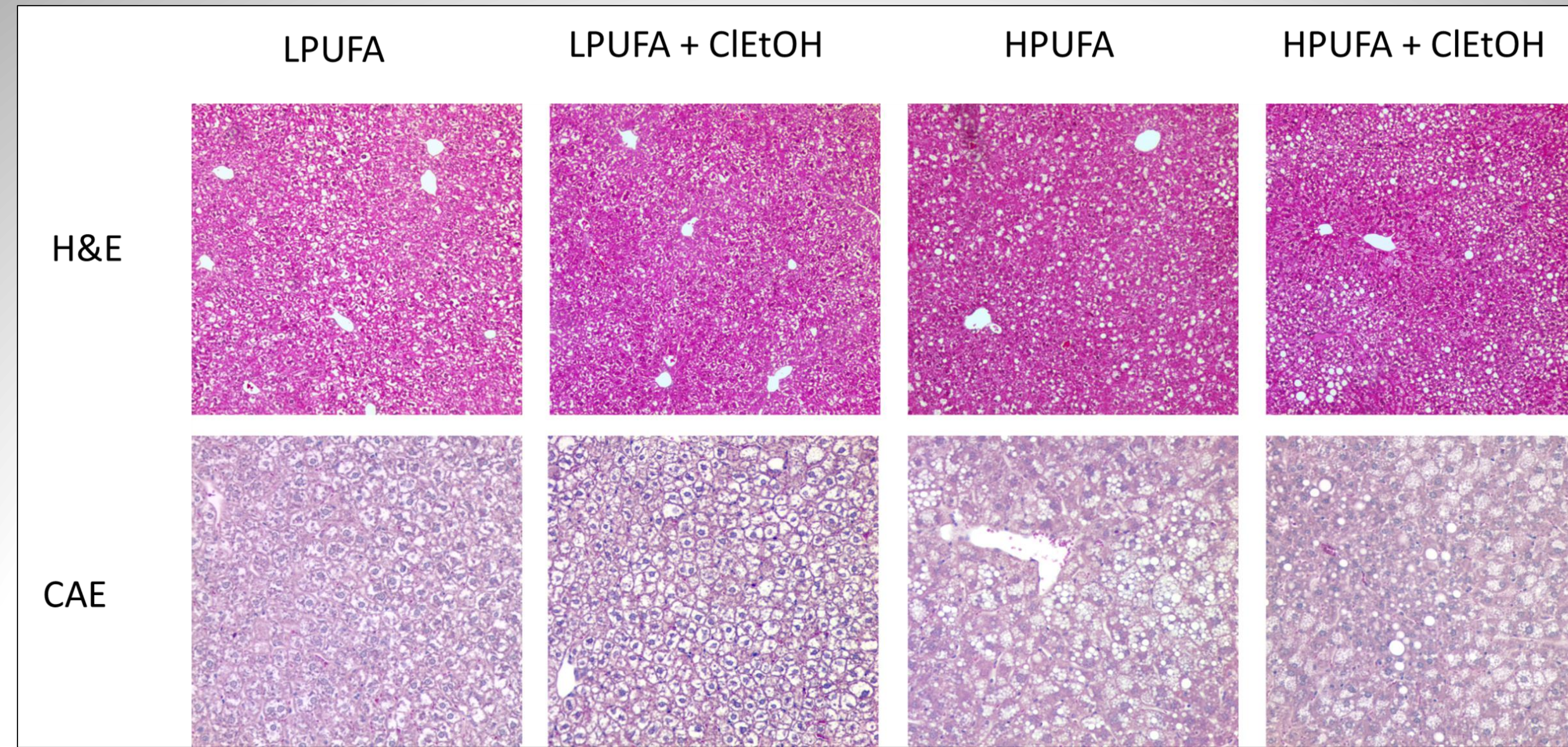


Figure 1: Mice were treated as described in *Materials and Methods*. Representative photomicrographs of hematoxylin & eosin (H&E) and chloroacetate esterase (CAE) are shown.

Whereas ClEtOH alone caused no changes in the livers of animals fed LPUFAs, it increased steatosis (macro- and microvesicular steatosis; H&E) and inflammation (CAE) in HPUFA fed animals.

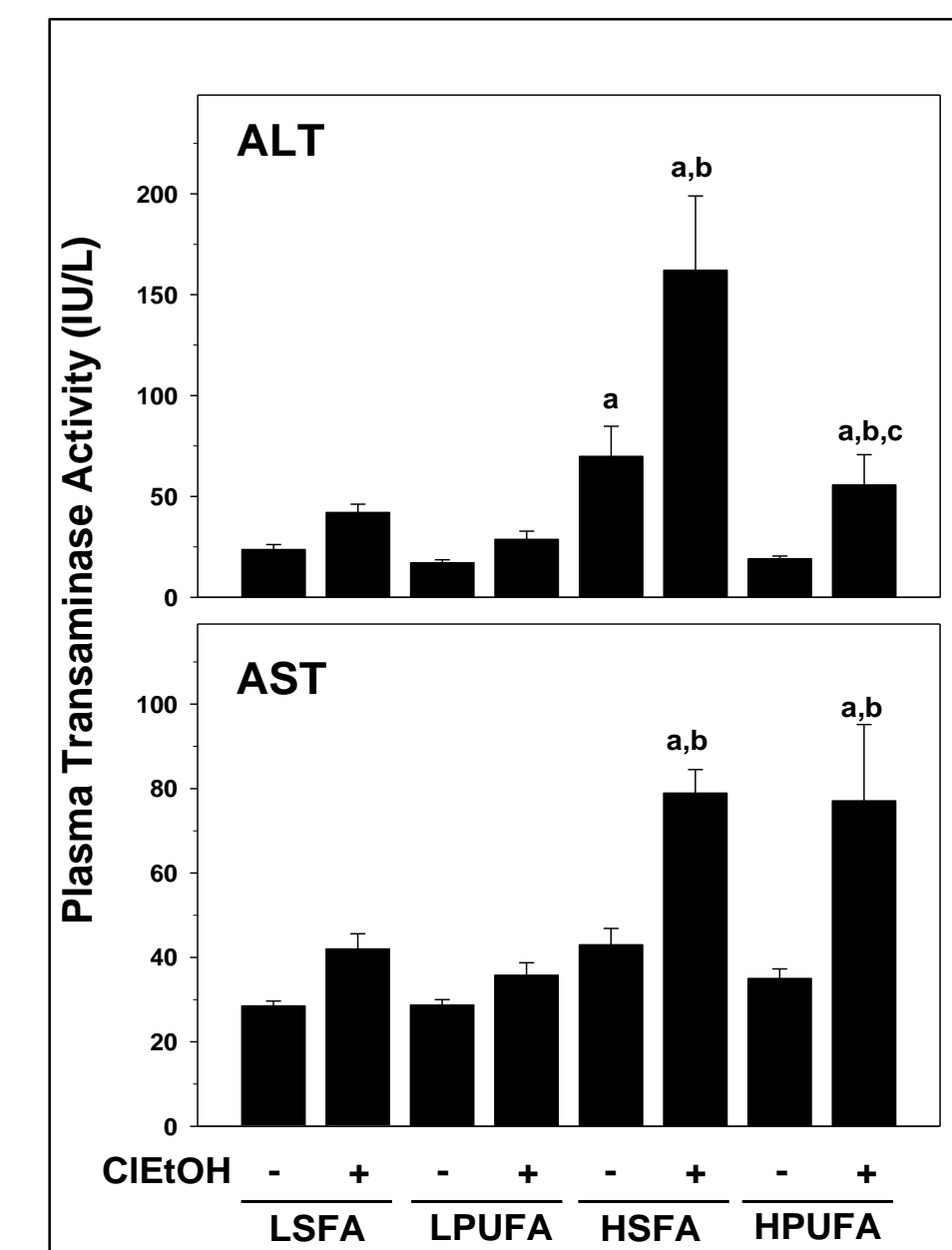


Figure 2: Injury due to the effects of ClEtOH. Mice were treated and real-Time RT-PCR for injury markers ALT and AST was performed as described in *Materials and Methods*.

ClEtOH significantly increased liver injury in the presence of HSFA. However, HPUFA partially blunted this effect.

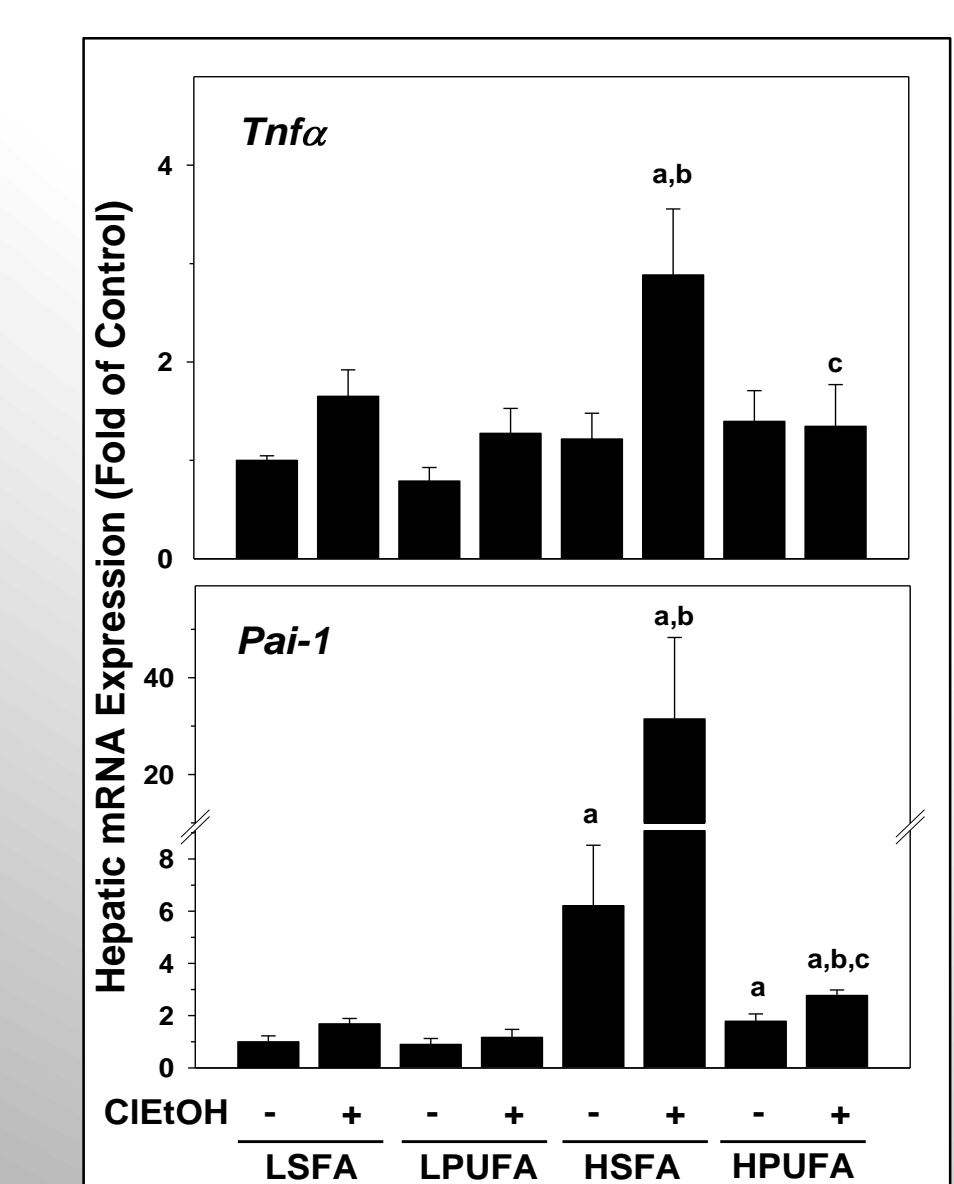


Figure 3: Effects of ClEtOH on inflammation in hepatic cells. Mice were treated as described in *Materials and Methods* and real-Time RT-PCR for inflammation markers *Tnfa* and *Pai-1* were performed.

ClEtOH significantly increased markers of inflammation in the presence of HSFA. However, HPUFA partially blunted this effect.

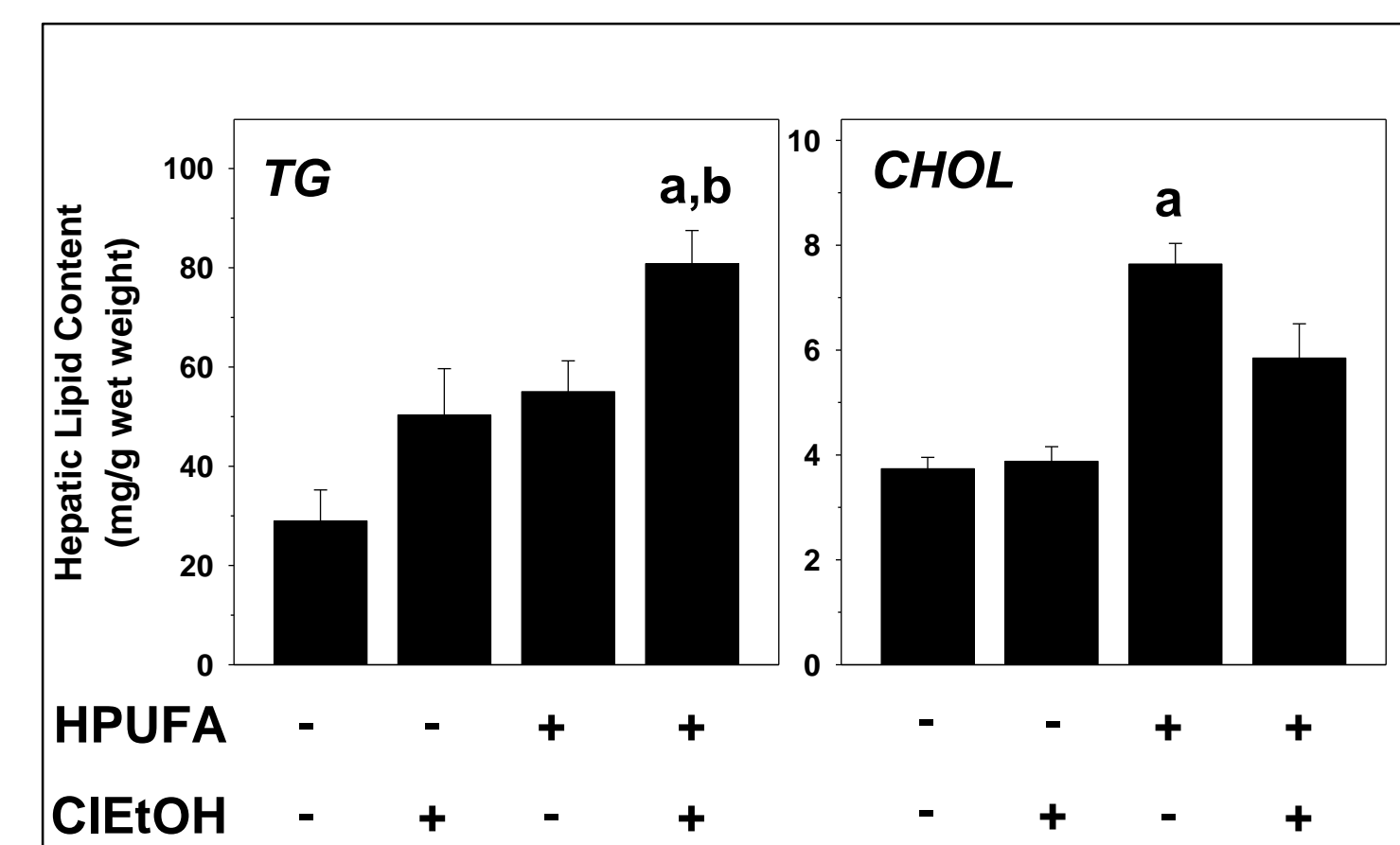


Figure 4: Effects of ClEtOH on Hepatic triglyceride and cholesterol content. Mice were treated and lipid extraction was performed on the liver samples as described in the *Materials and Methods*.

ClEtOH alone has no effect on hepatic lipid accumulation. A diet high in PUFAs increases both, hepatic TGs and Chol. Interestingly, ClEtOH further increases TGs but not Chol.

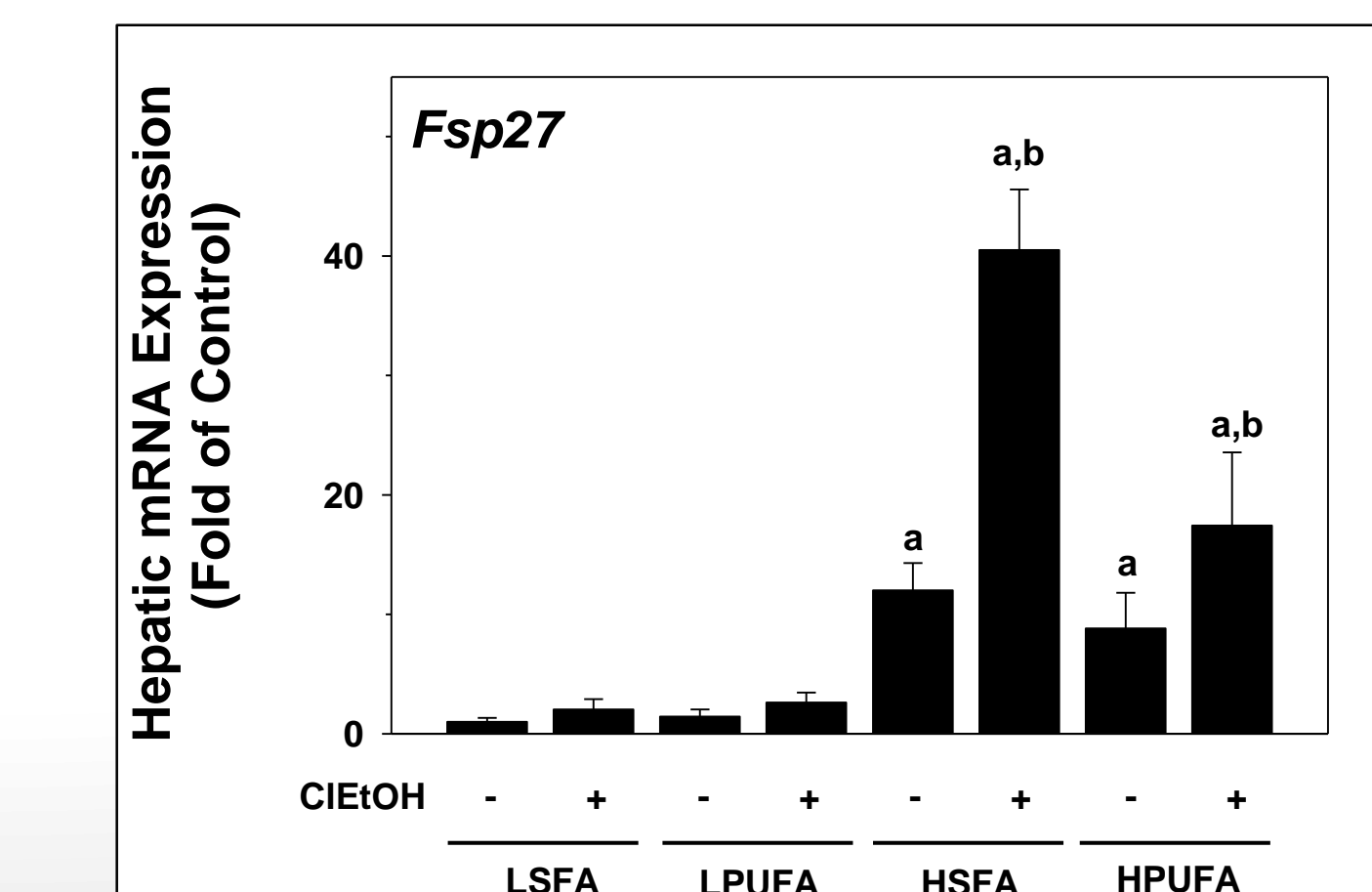


Figure 5: ClEtOH on Fsp27. Mice were treated and real-Time PCR for *Fsp27* were performed.

In HSFA + ClEtOH there is an enhancement of expression over the HSFA alone. There is a similar trend in the HPUFA groups but the response is attenuated. This suggests that HPUFAs may be protective against ClEtOH exposure.

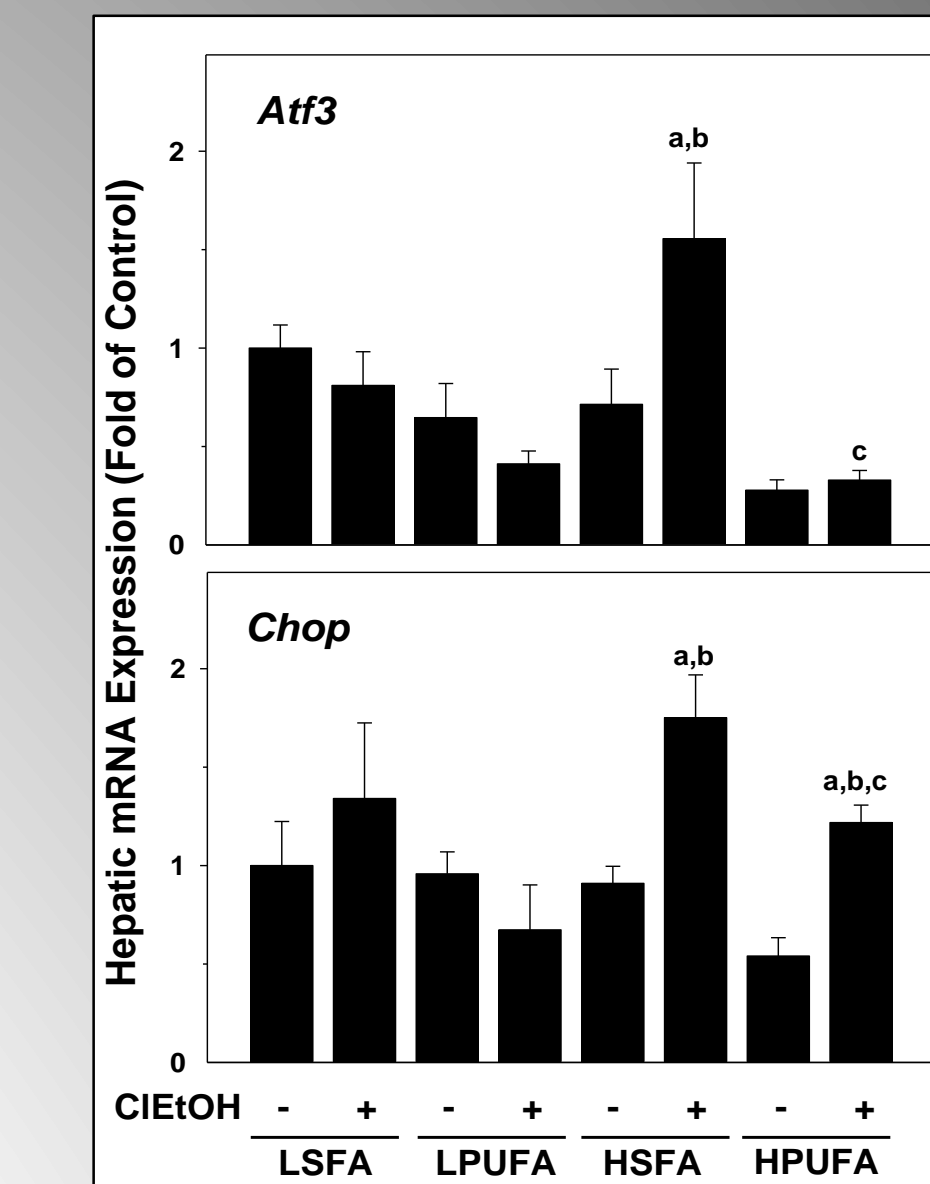


Figure 6: The influence of ClEtOH on ER stress in liver cells. Mice were treated and real-Time PCR for ER-stress markers *Atf3* and *Chop* were performed.

ClEtOH significantly increased ER stress in the presence of HSFA. However, HPUFA partially blunted this effect.

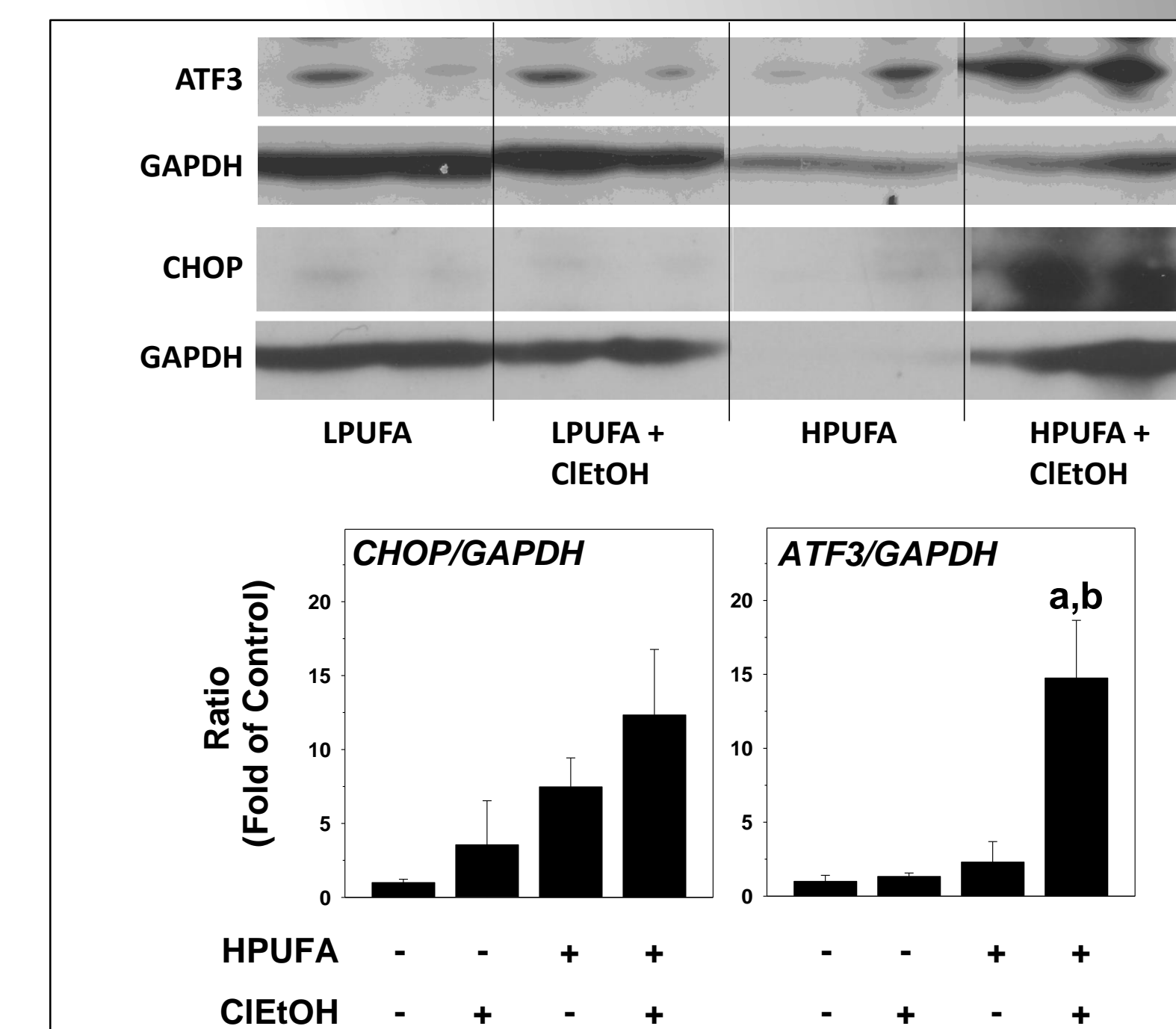


Figure 7: Effects of ClEtOH on ER-stress in liver extracts. Mice were treated and western blots for ER stress markers *CHOP* and *ATF3* were performed as described in *Materials and Methods*.

HPUFA-induced hepatic gene expression levels of ER stress markers was significantly increased by ClEtOH.

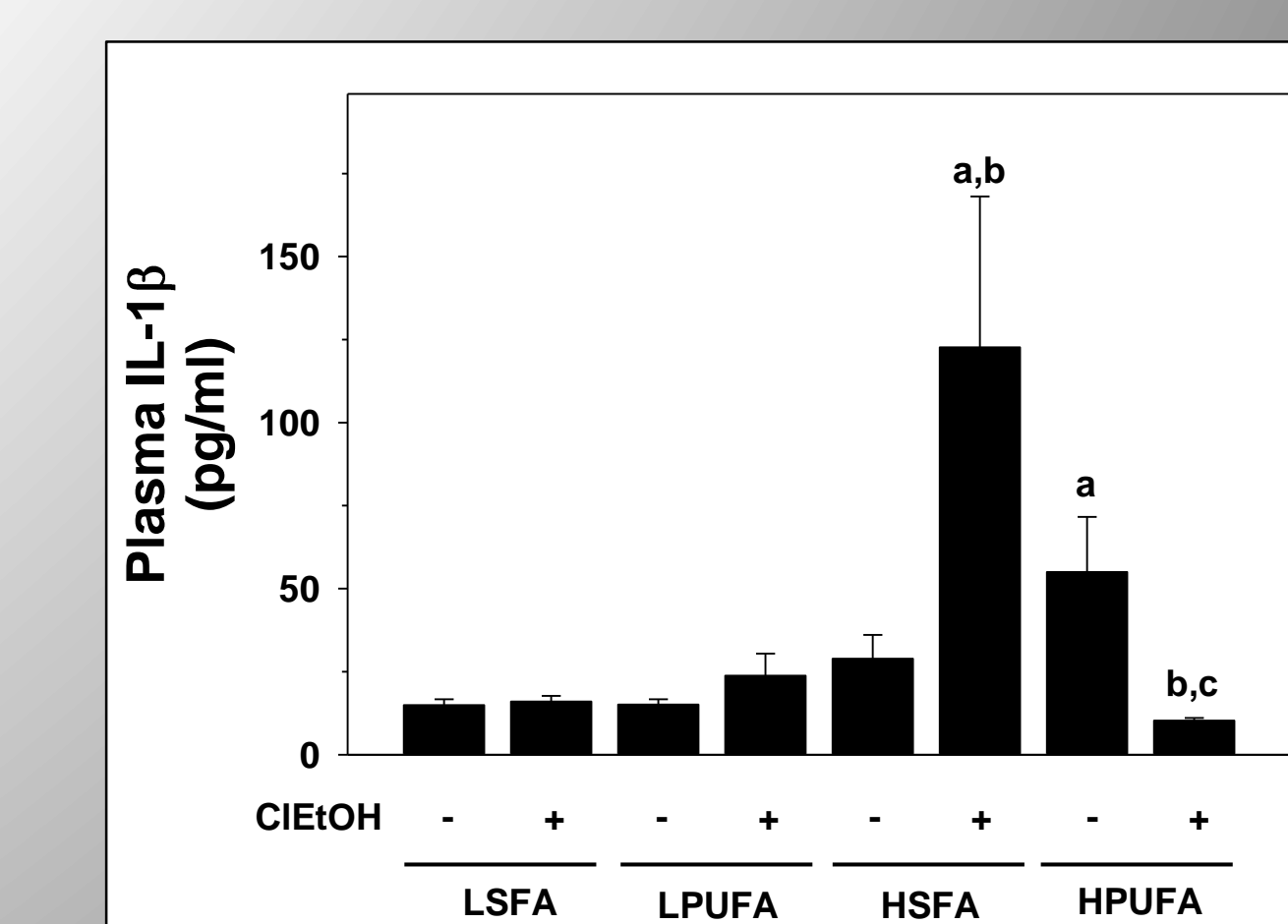


Figure 8: Inflammasome activity due to the effects of ClEtOH. An Elisa for IL-1β was performed on plasma samples from the treated mice.

Whereas ClEtOH significantly increased circulating IL-1β with HSFA, this effect was blunted in the presence of HPUFA, indicating that inflammasome activation was blunted in this group.

SUMMARY

Dietary polyunsaturated fatty acids blunt:

1. Liver damage
2. Inflammation
3. Lipid accumulation (steatosis)
4. ER Stress after ClEtOH

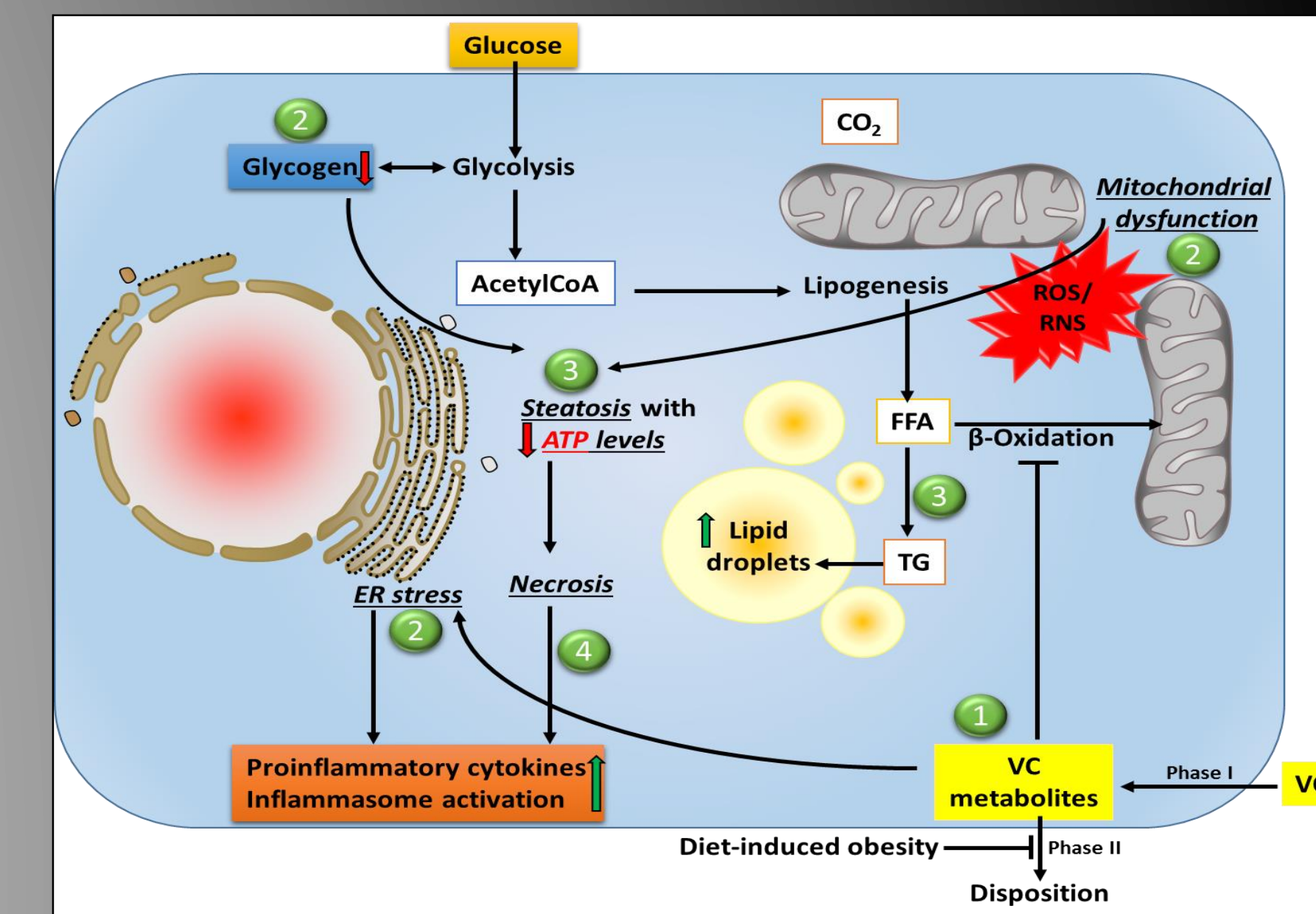


Figure 9: Working Hypothesis. Upon exposure to VC, 1) reactive solvent intermediates form through bio activation processes and diet-induced obesity decreases their elimination. 2) Through carbonyl stress and the generation of reactive oxygen and nitrogen species (ROS/RNS), solvent metabolites cause ER stress leading to the production of proinflammatory cytokines and mitochondrial damage, which impairs oxidative phosphorylation; the cell increases flux through anaerobic glycolysis to compensate for this loss of ATP yield. The increased demand for glucose depletes glycogen stores and the cell becomes 'pseudo-fasted'; 3) acetylCoA is being shunted to lipid synthesis (causing steatosis) rather than β-oxidation, even under conditions of ATP depletion. 4) The combined metabolic stress of solvent metabolite exposure and ATP depletion likely causes 'liponecrosis' associated with increased proinflammatory cytokines and inflammasome activation.

FUNDING SUPPORT

This research was supported in part by NCI (R25-CA134283 - BK), NIDDK (JIB; CJM), NIEHS (MC), NIAAA (CJM), and the Veterans Administration (MC, CJM).

REFERENCES

1. Cave, M., Deaciuc, I., Mendez, C., Song, Z., Joshi-Barve, S., Barve, S. & McClain, C. Nonalcoholic fatty liver disease: predisposing factors and the role of nutrition. *J. Nutr. Biochem.* 18, 184-195 (2007).
2. Cave, M. et al. Toxicant associated steatohepatitis in vinyl chloride workers. *Hepatology.* 51:474-81 (2010).
3. Day, C.P. & James, O.F. Steatohepatitis: a tale of two "hits"? *Gastroenterology.* 114, 842-845 (1998).
4. Flegal, K.M., Carroll, M.D., Ogden, C.L. & Curtin, L.R. Prevalence and trends in obesity among US adults, 1999-2008. *JAMA.* 303, 235-241 (2010).
5. Wang, X., Wang, S., Liu, Y., et al. The Hsp90 inhibitor SNX-2112 induces apoptosis of human hepatocellular carcinoma cells: the role of ER stress. *Biochemical and Biophysical Research Communications.* 446, 160-166 (2014).
6. Mohammad MK, Avila D, Zhang J, Barve S, Arteel G, McClain C, Joshi-Barve S. Acrolein cytotoxicity in hepatocytes involves endoplasmic reticulum stress, mitochondrial dysfunction and oxidative stress. *Toxicol Appl Pharmacol.* 265:73-82 (2012).

I3C Decreases Cyclin E Expression and Represses Cancer Cell Growth

Nicholas W. Kemper¹, Xiao-Mei Rao, M.D.^{2,5}, Stephen L. Wechman, B.S.^{3,5}, Heshan Sam Zhou, Ph.D.^{2,3,5}, Kelly McMasters, M.D., Ph.D.^{2,3,5}

University of Louisville¹; James Graham Brown Cancer Center²; Department of Pharmacology and Toxicology³; Department of Microbiology and Immunology⁴; Department of Surgery⁵
University of Louisville School of Medicine

Abstract

Introduction: A product of glucobrassicin breakdown; Indole-3-Carbinol (I3C) is one compound among several derived from cruciferous vegetables that have been identified for their anticancer effects. Previous studies have shown that I3C induces G₁ phase arrest, and works synergistically with Adenovirus to slow cancer cell replication and upregulate apoptosis, and may play a role in prevention and combination therapy for the treatment of tumors. Overexpression of cyclin E has been linked to tumorigenesis as it aids cell cycle transition into S phase where DNA replication can occur. ED1 cells have been transgenically induced to overexpress cyclin E causing tumorigenesis. Thus, ED1 mice should serve as a novel murine intermediate of cellular and human models, and serve as an effective in vivo model for Ad and I3C combination therapy.

Methods: In order to investigate the preventative and therapeutic potential of I3C, the current study utilizes MTT assay, crystal violet staining, and immunoblot analyses to understand the effect of I3C on cancer replication.

Results: I3C inhibits cell proliferation and metabolic activity in a dose-dependent manner. I3C also downregulates the expression of cell cycle proteins cyclin E, CDK2, and pRb.

Conclusion: I3C downregulates the expression of cell cycle proteins, which inhibits the proliferation of cancer cells. ED-1 cells are particularly susceptible to I3C treatment and should serve as a good model for the effects of I3C on human-type cyclin E in a murine model.

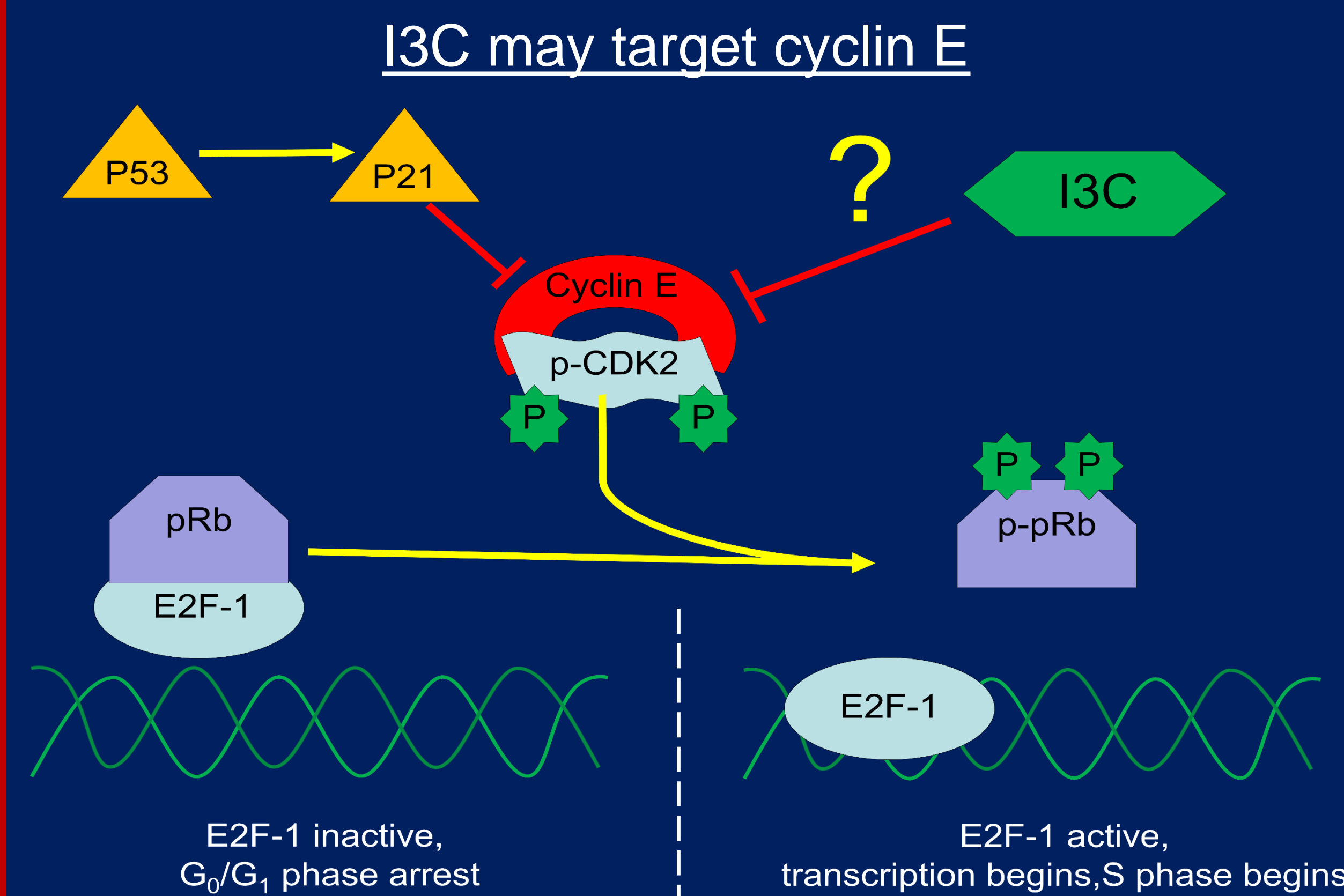


Figure 1: Diagram of I3C effect on cyclin E. I3C may induce G₁ arrest by targeting cyclin E or upstream regulators.

Results

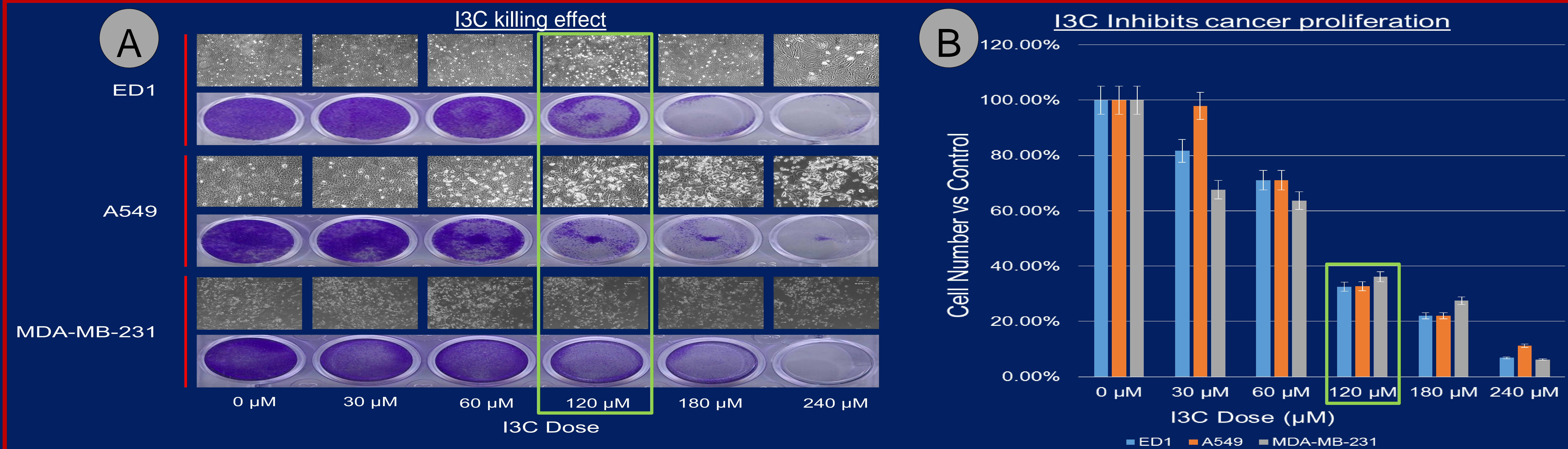


Figure 2: (A) Crystal violet stain and dose response. Cell pictures were obtained 3 days after treatment with respective dose of I3C, prior to crystal violet staining. After solubilizing, absorbance was read at 570 nm. **(B) Graph of absorbance vs increasing I3C dose.** Graph comparing absorbance across cell lines, with controls standardized to 100%.

I3C downregulates cyclin E, CDK2, and pRb

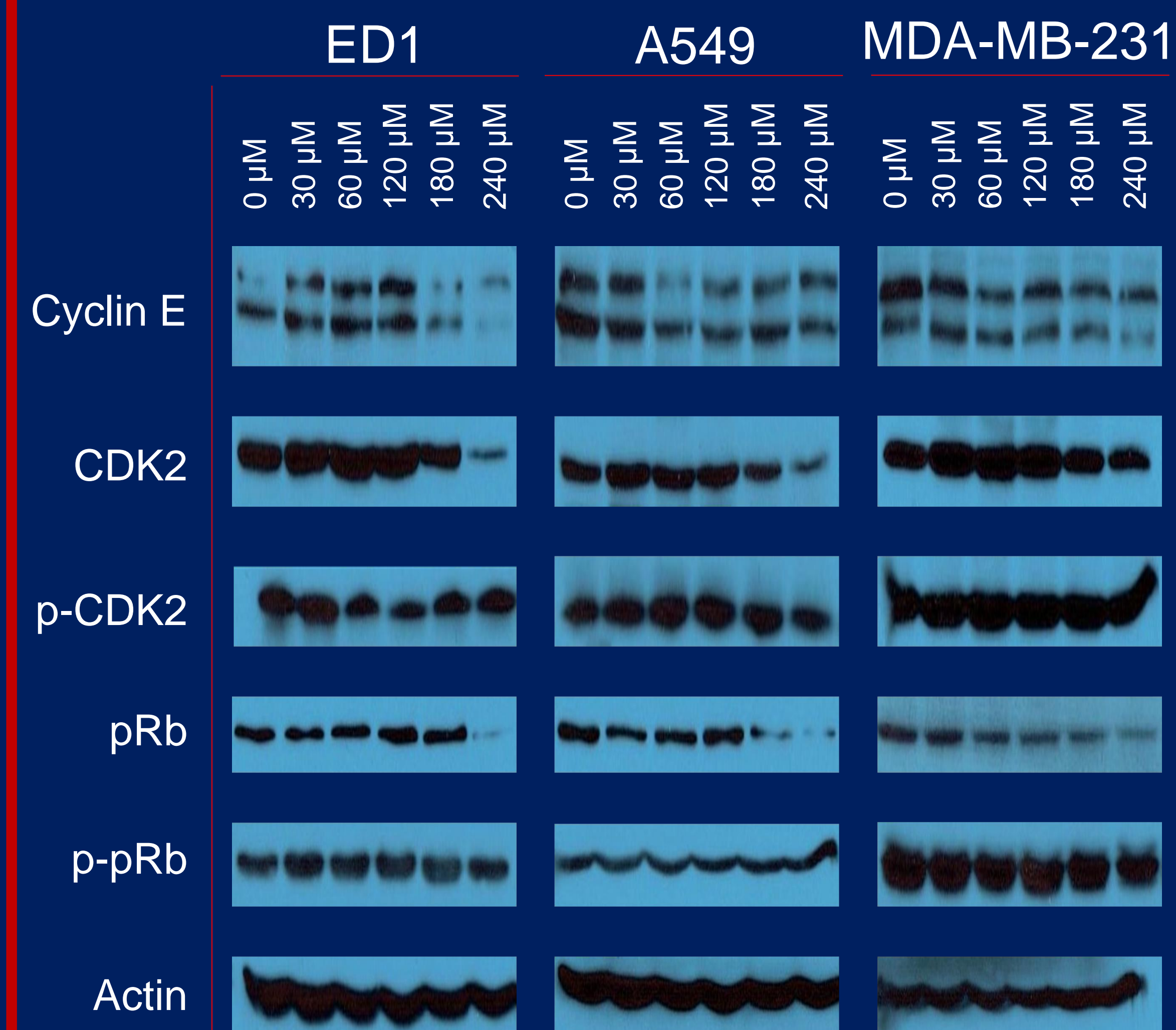


Figure 3: Effect of I3C on cell cycle protein expression. Cyclin E expression was tested along with CDK2, pRb, and their phosphorylated isoforms, with actin for loading control. Protein samples were isolated from cells 3 days after treatment with I3C.

I3C Inhibits cancer proliferation

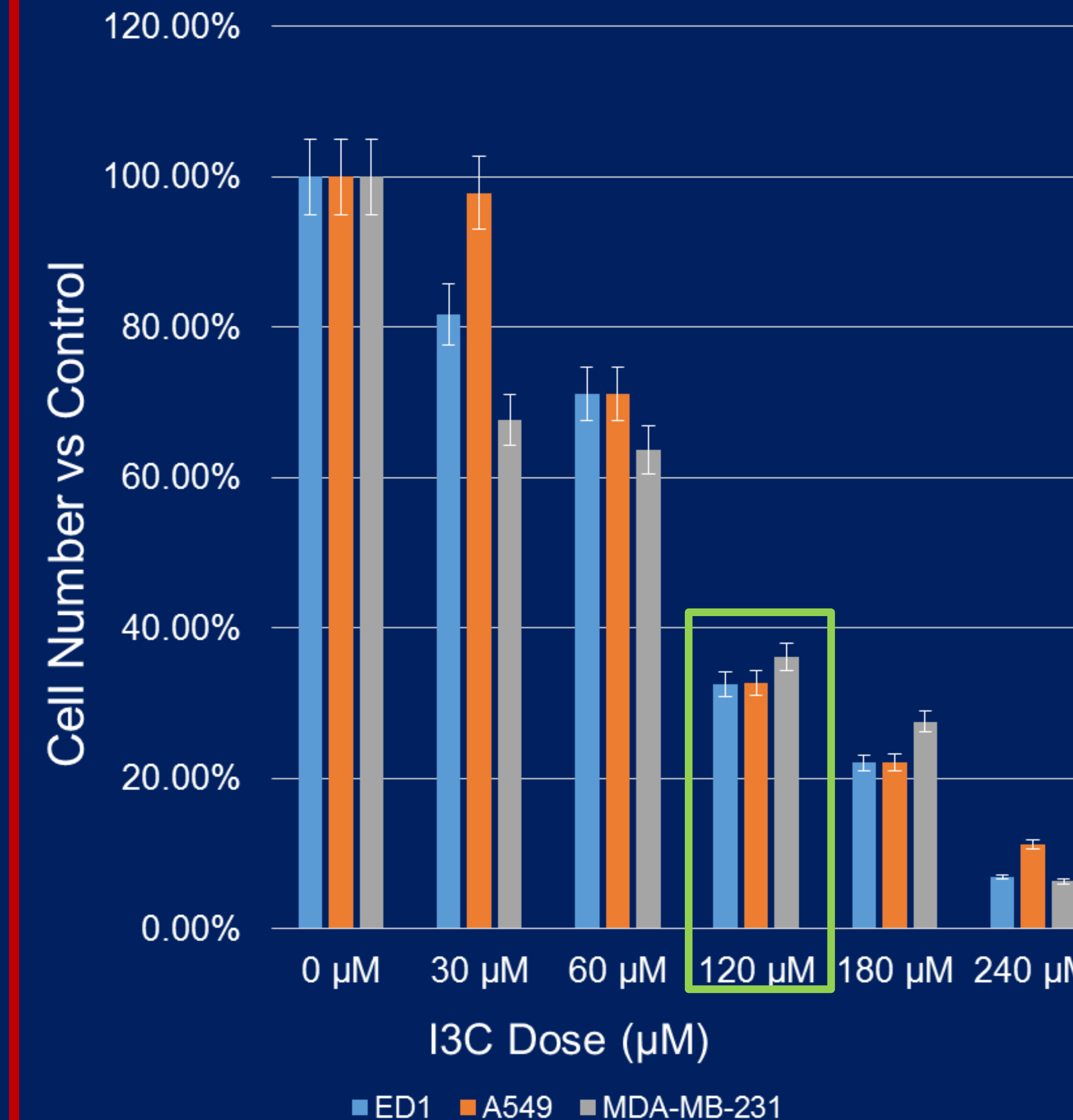


Figure 4: Relative metabolic activity of cells in response to I3C. Metabolically active cells produced purple formazin in response to MTT reagent.

Conclusions

- Cyclin E-overexpressed ED1 cells are most sensitive to I3C
- I3C represses cancer cell growth at high concentrations
- I3C downregulates cyclin E, CDK2, pRb

Future Directions

- Kinase activity assay
- Cell cycle proteins
- CDK1 activity
- Murine models with Ad infection

Acknowledgements

Research supported by a grant from the National Cancer Institute R25-CA134283, a grant from the Kentucky Lung Cancer Research Program (H. Sam Zhou), and the School of Medicine Summer Research Scholar Program.